CHAPTER V

MODEL SIMULATED CLIMATE CHANGES

A.   Introduction

The Mount Pinatubo volcanic eruption brought the largest amount of gaseous SO_2 into the stratosphere in this century.   The thermal, dynamical and chemical responses of the earth–atmosphere system to this perturbation of atmospheric constituents are complicated. Sulfate aerosol particles, converted from the gaseous SO_2, reflected solar radiation back into space in the ultra–violet and visible bands and absorbed part of the solar radiation in the near–infrared band. They also absorbed the upwelling terrestrial radiation.   As shown in Figs. 3.9 and 3.10, radiative–flux changes caused by the Pinatubo aerosol led to radiative heating in the stratosphere and radiative cooling in the troposphere.   Large atmospheric temperature and circulation anomalies were observed after the Pinatubo eruption.   However, not all the observed atmospheric temperature and circulation changes can be explained by the Pinatubo eruption.   Other external radiative forcings by, for instance, the increasing concentrations of atmospheric greenhouse gases and anthropogenic sulfate aerosol, and the internal variability of the earth–atmosphere system such as El Niños and the Quasi–Biennial Oscillation (QBO), also contributed to the observed temperature and circulation changes. El Niño events, which are not necessarily related to volcanic eruptions, often occur around volcanic eruptions (Robock and Mao 1995). The QBO influences the atmospheric responses to volcanic eruptions in two ways. First, it changes the transport of aerosol clouds in the tropics as a result of its phase change. Second, it causes a quasi–biennial oscillation of temperature in the tropical lower stratosphere (Angell 1997b) and a quasi–biennial oscillation of total ozone in the tropics (Angell 1997a).

In addition to their thermal and dynamical impact on the atmosphere, volcanic eruptions also influence the composition and distributions of atmospheric constituents through: (1) heterogeneous chemical reactions on the surface of aerosol particles, (2) anomalous dynamical transport of constituents by volcano–induced anomalous circulation, and (3) the gaseous and heterogeneous chemical reactions that have temperature–dependent reaction rates and radiation–dependent photolysis rates (Kinnison *et al.* 1994; Tie *et al.* 1994). During a few years following the Pinatubo eruption the observed total ozone decreased by more than 10% in the high latitudes of both hemispheres in springtime, and more than 2% in the tropics (Randel *et al.* 1995). These observed ozone losses must have caused further changes in atmospheric temperature and circulation.

The complicated interactions among all the components make it impossible to understand the influence of the Pinatubo eruption on climate by performing only observational data analyses. Numerical models with varying complexities in atmospheric dynamics, aerosol microphysics, radiative transfer and atmospheric chemistry have been used to study the Pinatubo eruption with focuses on one or a few components. No numerical models with all the components included have been used because of the complexity of the problem.

One group of numerical studies is focused on the formation and evolution of the Pinatubo volcanic aerosol cloud. To simulate the fate of the Pinatubo aerosol, Zhao *et al.* (1995) used a one–dimensional model with detailed gas–phase sulfur photochemistry, gas–to–particle conversion of sulfur, and aerosol microphysics such as condensational growth, coagulation and gravitational sedimentation. Bekki and Pyle (1994) used a two–dimensional chemical–radiative–dynamical model with detailed aerosol microphysics, but with gas–phase sulfur photochemistry ignored. Pudykiewicz and Dastoor (1995) used a three–dimensional spectral dynamical model with the transport of trace species explicitly resolved, but with highly

simplified sulfur chemistry and aerosol microphysics. These studies captured the basic features of the Pinatubo aerosol cloud, but all had obvious discrepancies from observations because of various model limitations.

Another group of numerical studies is focused on the simulation of atmospheric constituents after the Pinatubo eruption. For example, Kinnison *et al.* (1994) used a two–dimensional chemical–radiative–transport model to study the observed ozone depletion after the Pinatubo eruption. Observed aerosol optical data and aerosol surface area density were prescribed in the model. This model has detailed gaseous and heterogeneous chemistry. Influences of the atmospheric temperature and/or circulation changes induced by volcanic–aerosol heating on the simulated ozone losses were examined. Xie *et al.* (1994) used a two–dimensional chemical–dynamical–radiative model to simulate the evolution of post–Pinatubo chemical components, including ozone. Aerosol microphysics was included in their model to explicitly simulate the formation and evolution of aerosol cloud. Dynamical, radiative and chemical effects on the simulated ozone depletion were examined. Recently, Knight *et al.* (1998) simulated the Antarctic ozone hole for the two southern–hemisphere spring seasons following the Pinatubo eruption using a three–dimensional stratospheric model with simplified dynamics, but rather detailed radiative transfer and photochemistry. All the three models captured qualitatively the observed ozone depletion at certain times and at certain locations, but none of them could obtain a global solution comparable to the observations. It is still a great challenge for modelers to simulate correctly the formation and evolution of volcanic aerosol cloud and its impact on atmospheric constituents.

The third group of numerical studies is focused on the simulation of atmospheric temperature and circulation changes by using atmospheric GCMs with prescribed aerosol optical properties and without atmospheric chemistry. One of the earliest GCM studies was carried out

by Hansen *et al.* (1992). They coupled the GISS GCM, which has a coarse horizontal resolution of 8 by 10 degrees and only 1–2 layers in the stratosphere, to a non–dynamic mixed–layer ocean model with diffusive heat transport to the deeper ocean to simulate the surface temperature changes induced by the Pinatubo eruption. They used the volcanic aerosol optical depths of El Chichón with scaling to represent the Pinatubo eruption. There were no realistic dynamical interactions between the troposphere and the stratosphere, the Pinatubo–aerosol radiative forcing was not accurately prescribed in the model, and the impact of El Niños between 1991 and 1993 was not included. Graf *et al.* (1993) investigated the relation between the northern–hemisphere circulation and surface–air temperature anomalies after the Pinatubo eruption by performing perpetual–January simulations using the ECHAM2 GCM. They included the radiative forcing of volcanic aerosol in the model by reducing solar radiation at the model top (10 hPa) and adding externally computed heating rate anomalies in the stratosphere. They concluded that the observed continental warming in winter in the northern–hemisphere high latitudes is associated with the observed stronger–than–normal polar stratospheric vortex, which might have been caused by the anomalous radiative heating in the tropical lower stratosphere by the volcanic aerosol. However, the change in strength of the polar stratospheric vortex might also occur in the absence of volcanic aerosol forcing (Perlwitz and Graf 1994). Using the ECHAM2 GCM, Kirchner and Graf (1995) also performed a set of perpetual–January simulations to separate the signals of El Niño and volcanic aerosol forcing in the observed wintertime temperature and circulation.

Though the Pinatubo eruption has been the best observed volcanic eruption in history, the observational database on its own is still not adequate enough for GCM studies. Aerosol optical properties created for the Pinatubo eruption based on the limited observations of El Chichón eruption had been used in earlier GCM studies (Graf *et al.* 1993; Hansen *et al.* 1996; Kirchner and Graf 1995). In this study, we constructed a two–dimensional, time–dependent, zonally averaged,

vertically resolved spectral dataset of the Pinatubo aerosol optical properties, covering the time from June 1991 through May 1993, for the UIUC 24–layer ST–GCM. This dataset has been described in detail in Chapter III and by Andronova *et al.* (1999). It provided us the best–possible characterization so far of the Pinatubo aerosol optical properties. In this chapter we use this dataset in the UIUC 24–layer ST–GCM to simulate and understand the atmospheric temperature and circulation changes induced by the Pinatubo eruption. The 24–layer ST–GCM can resolve aerosol radiative forcing explicitly in both the solar and terrestrial bands. It has rather fine spectral–resolution radiation bands and a sophisticated radiative–transfer scheme (Appendix A). Since the model's top is at 1 hPa, it can better resolve the part of the aerosol cloud that extended into the upper stratosphere that was not well represented by earlier studies. We performed a few sets of ensemble simulations using the UIUC 24-layer ST–GCM with prescribed sea–surface temperature (SST), and using the coupled 24–layer–atmosphere/18–layer–ocean GCM. Atmospheric chemistry is not considered in any of the simulations. We examine here the sensitivity of the simulated climate changes induced by the Pinatubo aerosol to atmospheric initial conditions, sea–surface temperature and sea–ice distributions, and the thermal inertia of the ocean. We compare the simulated results with observations to test the model's strengths and weaknesses in simulating the observed atmospheric temperature and circulation changes related to the volcanic aerosol forcing, and explore the effects of El Niño, ozone depletion and the Quasi–Biennial Oscillation on the simulated climate changes. It should be indicated that at the time of writing this thesis, we were informed that recently Kirchner *et al.* (1999) also performed a set of numerical experiments to study the climate responses of the atmosphere to the Pinatubo eruption. They used the ECHAM4 GCM, which can resolve aerosol radiative forcing explicitly. They performed three sets of 2–year–long ensemble simulations, with and without the volcanic aerosol forcing, with three different SSTs: climatological SST, El Niño–type SST of 1991~1993 and La Niña–type SST

of 1984~1986. They tested their model's ability to reproduce the observed climate changes induced by the Pinatubo aerosol with different SSTs.

Section B outlines the ensemble simulations performed by the 24–layer ST–GCM. Section C presents the simulated results of the ensemble simulations. The simulated results are compared to observations. A statistical model is used in Section D to estimate the influence of the QBO on the observed temperature anomalies in the tropical lower stratosphere. Section E estimates the influence of the observed ozone depletion on the simulated temperature anomalies. Section F presents the temperature anomalies induced by the Pinatubo eruption simulated by the UIUC coupled 24–layer–atmosphere/18–layer–ocean GCM. Section G summarizes this chapter.

B.   Design of the Ensemble Simulations

Using the UIUC 24–layer ST–GCM, we performed four sets of ensemble simulations (see Table 5.1). Each set contains 6 simulations that use different initial conditions, and each simulation spans two years from June 1991 through May 1993. All the simulations used the AMIP–II climatological SSTs (CSST) or real–time SSTs (RSST) and the AMIP–II climatology of ozone concentration (Gleckler 1999). The climatological SSTs are the 17-year averages of the data from 1979 through 1995. The real–time SSTs are monthly means from June 1991 through May 1993. One El Niño event occurred between March 1991 and July 1992, and the other between February 1993 and September 1993 (Trenberth 1997). The Pinatubo aerosol was introduced into the model by using the zonally averaged, time–dependent monthly mean aerosol optical properties (extinction efficiency, single–scattering albedo and asymmetry factor) described in Chapter III. A set of six different initial conditions for starting the model simulations on June 1 were picked randomly from a 15–year control simulation of the 24–layer ST–GCM (Appendix A). The four sets of ensemble simulations listed in Table 5.1 used the same set of initial conditions.

The difference between any two simulations, which start from the same initial condition and belong to two different sets of ensembles, is calculated. The average of the six differences between two sets of ensembles is defined as the ensemble mean of an experiment. We list in Table 5.2 the experiments that we construct from the four sets of ensemble simulations in Table 5.1. A label is assigned to each experiment starting with SI, which means simulation and is used to distinguish itself from observation (OB) in the following analyses.

Table 5.1. *Ensemble simulations performed by the 24–layer ST–GCM.*

Ensemble Simulations	Prescribed SSTs	Including the Pinatubo Volcanic Aerosol (VOL) ?
E1	CSST	no
E2	CSST	yes
E3	RSST	no
E4	RSST	yes

Table 5.2. *Experiments and climate changes induced by the Pinatubo aerosol and/or SSTA.*

Experiments	Differences	Climate Changes Induced by
SI:VOL/CSST	E2 – E1	the Pinatubo aerosol simulated with climatological SST
SI:VOL/RSST	E4 – E3	the Pinatubo aerosol simulated with real–time SST
SI:VOL+SSTA	E4 – E1	both the Pinatubo aerosol and SST anomalies
SI:SSTA	E3 – E1	SST anomalies without the Pinatubo aerosol
SI:SSTA/VOL	E4 – E2	SST anomalies with the Pinatubo aerosol

C. Results of the Ensemble Simulations and Comparison with Observations

1. Surface–Air Temperature Anomalies

In Chapter IV, we analyzed the observed surface–air temperature anomalies (ΔT_s) and applied the Singular Value Decomposition (SVD) method to quantify and separate the contributions of SST anomalies in the tropical Pacific from the observed continental ΔT_s. We examine now how well the 24–layer ST–GCM simulates the observed continental ΔT_s when forced by the Pinatubo aerosol radiative forcing and/or SST anomalies. Fig. 5.1a shows the seasonal–mean ΔT_s from JJA 1991 through MAM 1993 averaged over the four continents (Eurasia, North America, South America and Africa) for the simulated ensemble mean when the model is forced by the Pinatubo aerosol forcing and SST anomalies (Experiment SI:VOL+SSTA), and for the high–pass–filtered observations with time scales less than 120 months (OB:HPF). Fig. 5.1b shows the seasonal–mean continental ΔT_s for the simulated ensemble means when the model is forced only by SST anomalies, with (Experiment SI:SSTA/VOL) and without (Experiment SI:SSTA) the Pinatubo aerosol included in both the control runs and the perturbation runs, and for the projections of the leading mode of the observed ΔT_s (OB:SVDP1), which is the part of observation explained by the SST anomalies in the eastern tropical Pacific. Fig. 5.1c shows the seasonal–mean continental ΔT_s for the simulated ensemble means when the model is forced only by the Pinatubo aerosol, with climatological SSTs (Experiments SI:VOL/CSST) and real–time SSTs (SI:VOL/RSST) as the lower boundary conditions in both the control runs and the perturbation runs, and for the difference between OB:HPF and OB:SVDP1, which includes the observed ΔT_s induced by the Pinatubo aerosol and forcings other than the SST anomalies. The correlation coefficients between the simulations and their corresponding observations are calculated and depicted in Fig. 5.1.
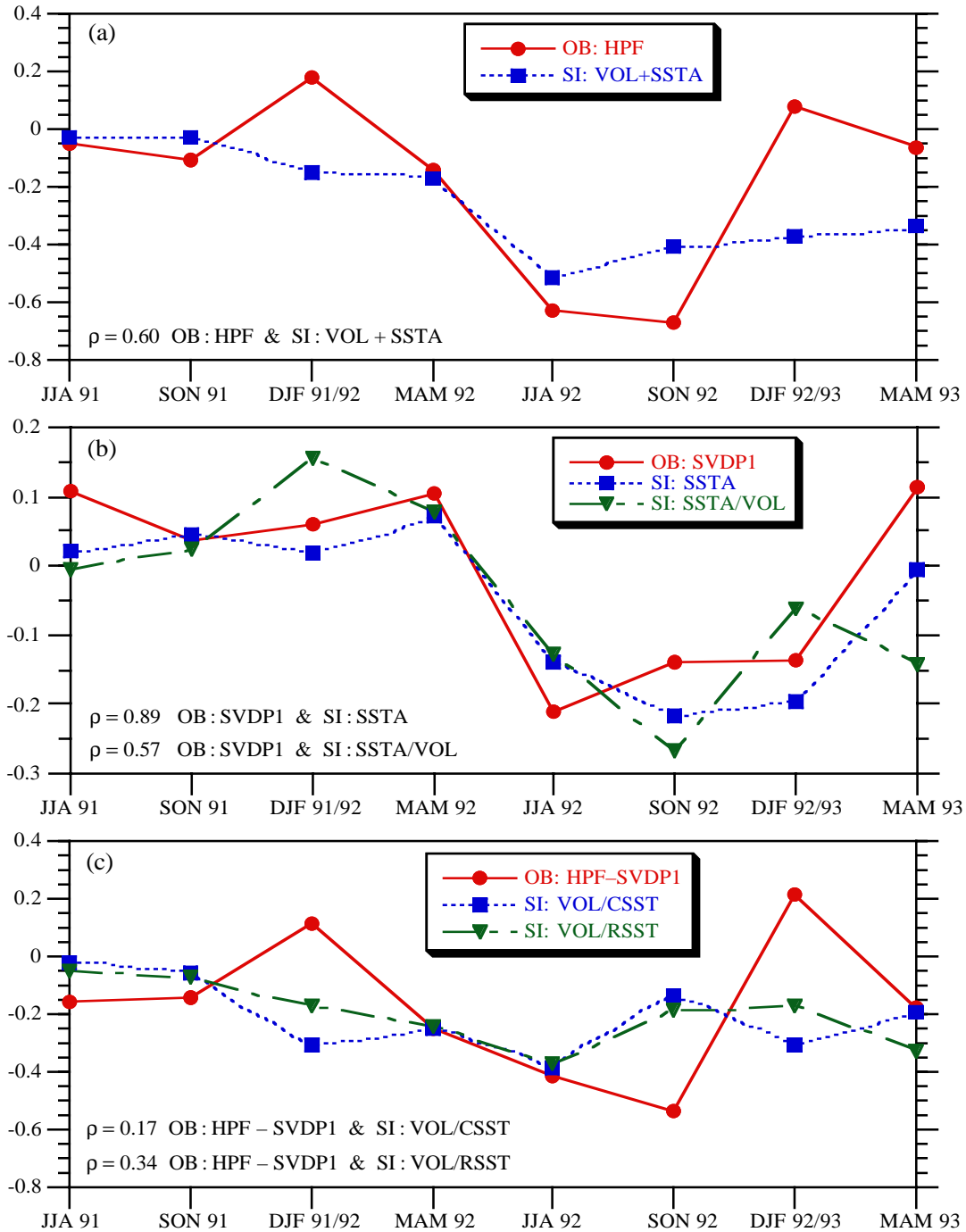
Fig. 5.1. *Seasonal–mean surface–air temperature anomalies (°C) averaged over the continents of Eurasia, North America, South America and Africa. The simulated results are ensemble means. Correlation coefficients between the simulations and their corresponding observations are shown at the lower-left corner of each figure. See the text and Table 5.2 for the meanings of the legends.*

Ideally, the lines in each figure should match each other in magnitude and phase if the model and the SVD tool had been perfect. From Fig. 5.1b we can see that, when forced only by SST anomalies, the model simulates rather well the observed global–mean continental ΔT_s that can be explained by the SST anomalies from the SVD analysis (OB:SVDP1). The ensemble without the Pinatubo aerosol included (SI:SSTA) simulates better the observed ΔT_s than the ensemble with the Pinatubo aerosol included (SI:SSTA/VOL). The correlation coefficients are 0.89 between the lines of OB:SVDP1 and SI:SSTA, and 0.57 between the lines of OB:SVDP1 and SI:SSTA/VOL. The simulated surface–air temperature over the four continents (T_s) increased from JJA 1991 to MAM 1992 by about 0.1°C, and decreased from MAM 1992 to SON 1992 by about 0.25°C. On the other hand, Fig. 5.1b also proves that the SVD analysis is capable of finding the coupled patterns between the continental ΔT_s and the SST anomalies in the eastern tropical Pacific. When forced by both the Pinatubo aerosol and SST anomalies (Fig. 5.1a), the model simulates rather well the observed global–mean ΔT_s in the northern–hemisphere spring and summer. The averaged surface–air temperature over the four continents decreased by 0.51°C in the simulation and by 0.63°C in the observation in JJA 1992, among which 0.14°C in the simulation (Experiment SI:SSTA) and 0.21°C in the observation (OB:SVDP1) are due to the SST anomalies. Unfortunately, the model failed to simulate the observed warming in DJF 1991–1992 and DJF 1992–1993. The simulated ΔT_s are negative. When forced only by the Pinatubo aerosol (Fig. 5.1c), the model simulates well the observed temperature anomalies in the northern–hemisphere spring and summer but rather poorly in the northern–hemisphere fall and winter seasons, no matter with climatological or real–time SSTs as the lower boundary conditions. The difference of the simulated continental ΔT_s between the two experiments SI:VOL/CSST and

SI:VOL/RSST is small, with the latter being closer to the observation in DJF 1991–1992 and DJF 1992–1993.

We further analyze the geographical distributions of surface–air temperature anomalies. In the following analyses we will exclude the Experiment SI:SSTA/VOL for two reasons. First, detailed analyses showed that the geographical distributions and magnitudes of the ensemble–mean temperature anomalies simulated by the Experiment SI:SSTA/VOL are similar to those by the Experiment SI:SSTA in both the troposphere and stratosphere in all seasons, and near the surface except in DJF 1991–1992. Second, the Experiment SI:SSTA/VOL represents virtually the difference between the Experiments SI:VOL/RSST and SI:VOL/CSST, which will be analyzed in detail. Fig. 5.2 presents the seasonal–mean surface–air temperature anomalies over the four continents in DJF 1991–1992 for the observational data analyses and the simulations listed in Fig. 5.1, except for the simulation SI:SSTA/VOL. A two–tailed t–test has been used to compute the statistical significance of the simulated ensemble–mean ΔT_s. Areas with statistical significance exceeding the 10% level are shaded. For the observations, areas with values exceeding 1.3σ in magnitude are shaded, where σ is the standard deviation of the high–pass–filtered seasonal–mean ΔT_s at each grid point between 1950 and 1997. For a time series with a normal distribution and with no auto–correlation, about 10% of the data fall outside of the range $\{-1.3\sigma, 1.3\sigma\}$. Therefore, the shaded areas are at about the 10% level of statistical significance. For the Experiment SI:VOL+SSTA, the model captured the large warming of about 3°C over central and northwestern North America and the cooling over northern Africa, where the observed temperature anomalies are significant (Fig. 5.2b). Over central Eurasia, the observed anomalies are about +2°C but not significant, and the model simulated anomalies are negative. For the Experiment SI:SSTA, the simulated ΔT_s over central North America are about 0.5°C to
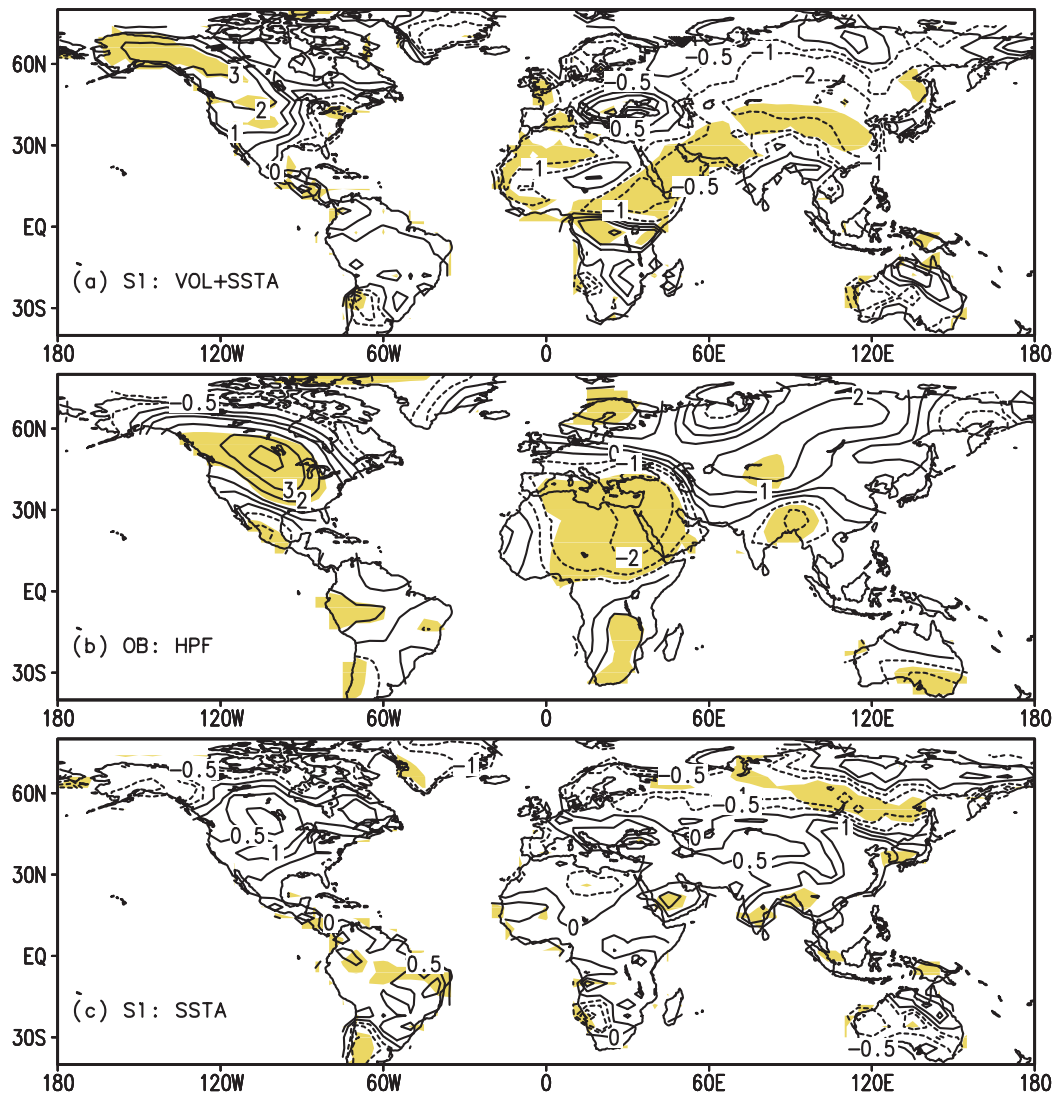
Fig. 5.2. *Geographical distributions of surface–air temperature anomalies over land in DJF 1991–1992. The contour interval is 1°C with the ±0.5°C lines added. Dashed lines are negative anomalies, and solid lines are positive anomalies. For the simulations in (a), (c), (e) and (f), shaded areas have statistical significance exceeding the 10% level for a two–tailed t–test. For the observations in (b), (d) and (g), shaded areas have temperature anomalies larger than 1.3σ in magnitude, where σ is the standard deviation of the high–pass–filtered seasonal–mean temperature anomalies at each grid point.*
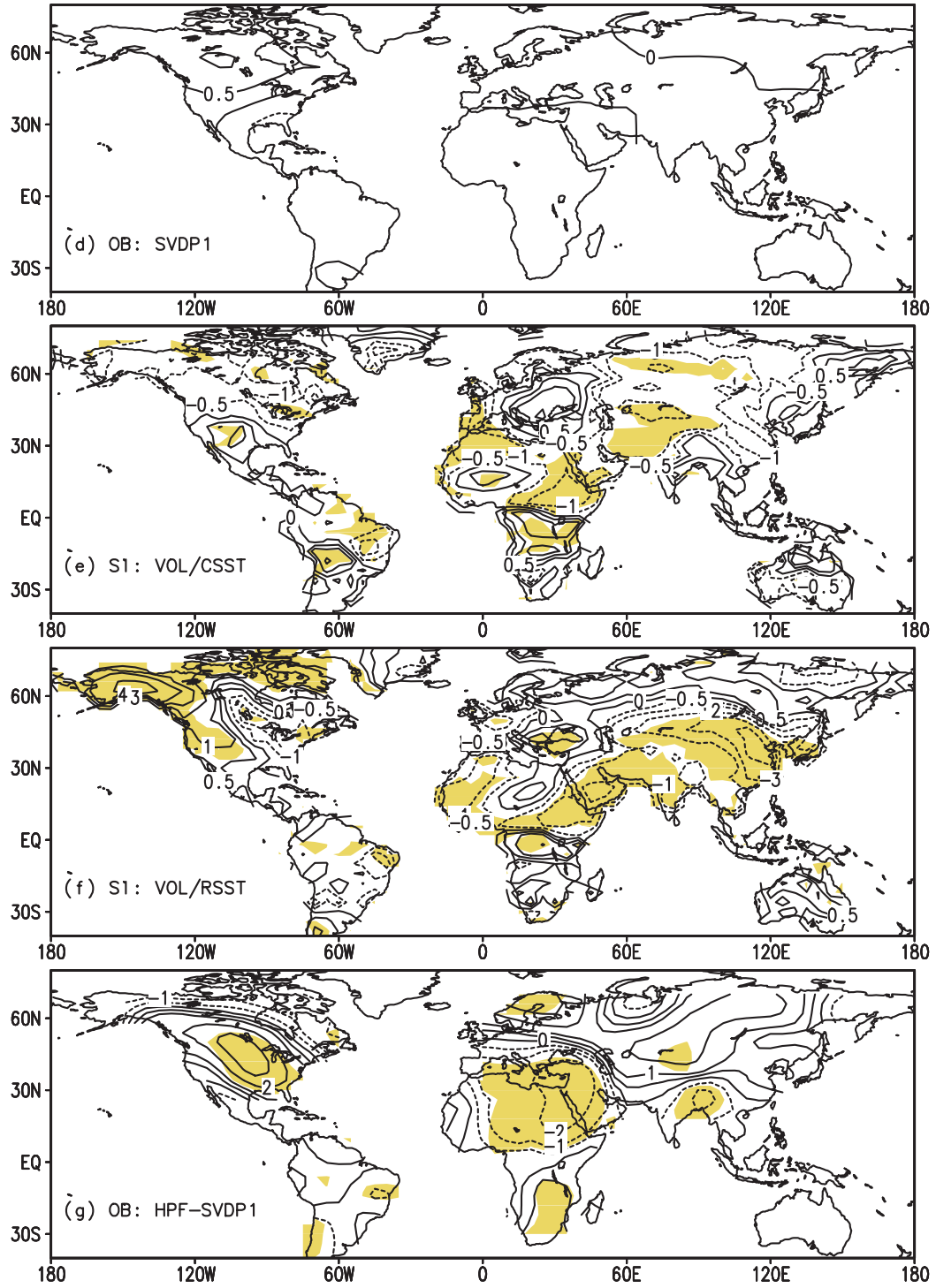
Fig. 5.2.   (*Continued.*)

1.0°C, and match the corresponding observations associated with the El Niño/La Niña modes derived from the SVD analysis (Fig. 5.2.d). For the Experiments SI:VOL/CSST and SI:VOL/RSST, the simulated ΔT_s do not match well the corresponding observations in Fig. 5.2g. A few points can be drawn from Fig. 5.2. First, for any set of ensemble experiment, the simulated ΔT_s are sensitive to their initial conditions. As a result, the simulated ΔT_s do not pass the 10% level of statistical significance over most continental regions as shown by the shadings in Fig. 5.2. Second, the natural variability of surface–air temperature is larger over Eurasia than over North America and Africa. The model performs better in regions where the observed ΔT_s are significant. Third, the ensemble experiment with both the SST anomalies and the Pinatubo aerosol forcing included (SI:VOL+SSTA) produces better results than the two ensemble experiments with only Pinatubo aerosol included. Fourth, when the model is forced only by the Pinatubo aerosol, the simulated ΔT_s does depend on the type of SSTs prescribed (Fig. 5.2e and f).

In JJA 1992 (Fig. 5.3), the simulated continental ΔT_s by each of the four experiments are all rather significant and match the corresponding observations generally well. Both the SST anomalies and the Pinatubo aerosol forcing contributed to the observed cooling over Eurasia and central North America.

We calculated the pattern correlation coefficients of surface–air temperature anomalies over Eurasia, North America, Africa and South America, respectively, between the ensemble means of each experiment and their corresponding observational data analyses for DJF 1991–1992 and JJA 1992. Accordingly, we also calculated the ratios of the area-averaged surface–air temperature anomalies between the ensemble means of each experiment and their corresponding observational data analyses for these regions. The calculated pattern correlation coefficients are rather small, and are even negative for some cases, for all four continents in both seasons. In

general, the results for Eurasia and North America are slightly better than those for Africa and South America. We present the results for Eurasia and North America in Table 5.3. For most cases, the pattern correlation coefficients are higher for JJA 1992 than for DJF 1991–1992, and higher for North America than for Eurasia. One can notice that in some cases the area–averaged surface–air temperature anomalies even have opposite signs between the simulation and the observation.
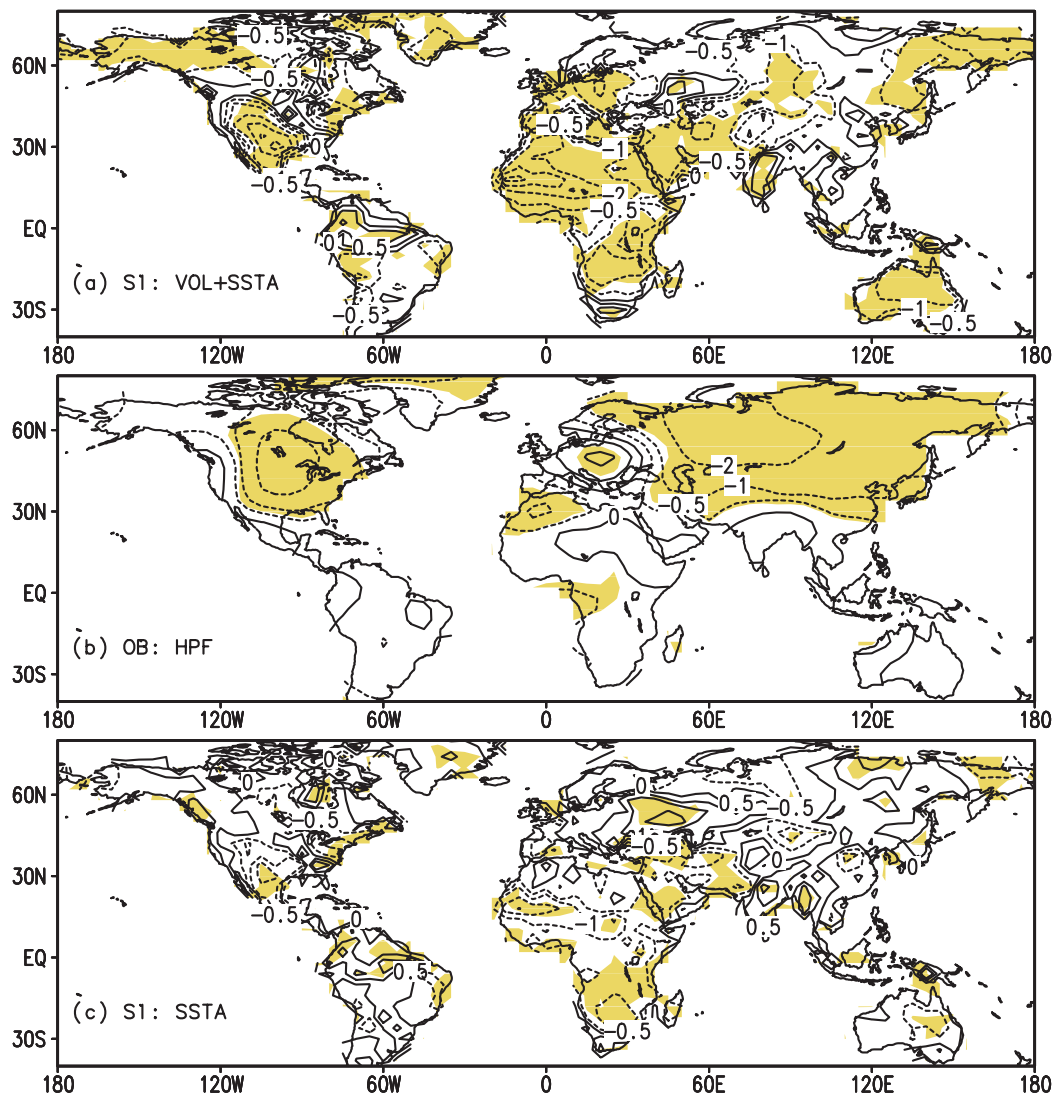
Fig. 5.3.   *As in Fig. 5.2, except for JJA 1992.*

(d) OB: SVDP1

(e) S1: VOL/CSST

(f) S1: VOL/RSST

(g) OB: HPF-SVDP1
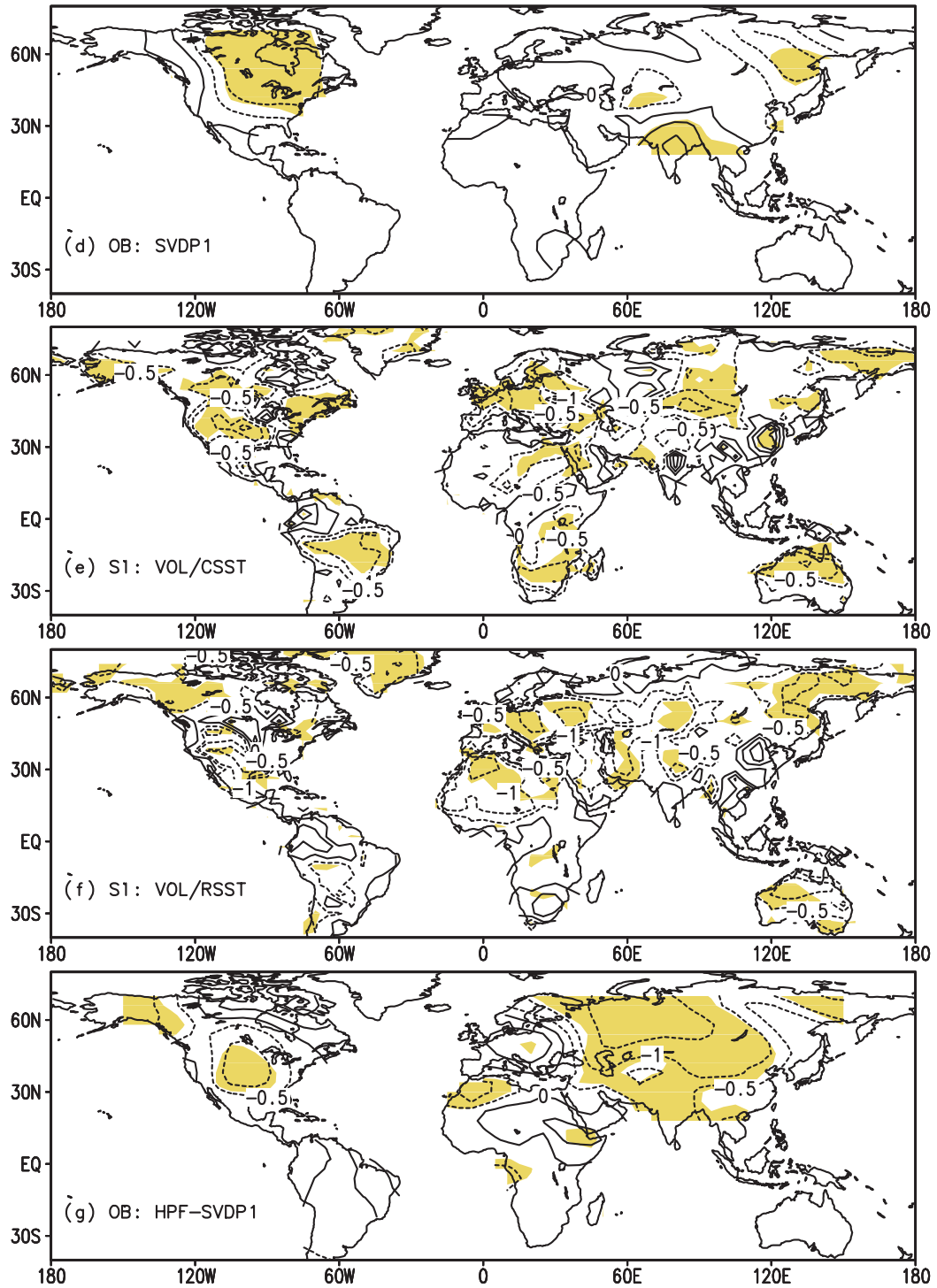
Fig. 5.3.   (*Continued.*)

Table 5.3. *Pattern correlation coefficients and the ratios of area–averaged surface–air temperature anomalies between the ensemble means of each experiment and the corresponding observational data analyses over Eurasia and North America, respectively, for DJF 1991–1992 and JJA 1992. The value at each grid point has been weighted by the area of the grid before use.*

Simulation versus observation	Eurasia				North America			
	Pattern correlation		Ratio (SI/OB)		Pattern correlation		Ratio (SI/OB)	
	DJF 1991/1992	JJA 1992	DJF 1991/1992	JJA 1992	DJF 1991/1992	JJA 1992	DJF 1991/1992	JJA 1992
SI:VOL+SSTA OB:HPF	–0.4422	0.2461	–1.7216	0.45634	0.3315	0.3422	0.93068	0.67095
SI:SSTA OB:SVDP1	0.3889	0.2462	12.048	–0.37014	0.3420	0.1987	0.50708	0.30855
SI:VOL/CSST OB:HPF – SVDP1	–0.4817	0.1316	–1.1154	0.48079	0.1188	0.5014	–0.80997	1.7462
SI:VOL/RSST OB:HPF – SVDP1	–0.2043	0.1323	–1.9120	0.62285	–0.1445	0.2904	1.1591	1.3286

The reasons for the different performance of the 24–layer ST–GCM in simulating the surface–air temperature anomalies in DJF and JJA can be summarized in three points. First, the natural variability of surface–air temperature over the northern–hemisphere high latitudes is larger in DJF than in JJA. The observed ΔT_s in DJF 1991–1992 over Eurasia might result from the natural variability. Second, in DJF 1991–1992 the observed warming over central Eurasia and North America might be caused by an anomalous troposphere–stratosphere exchange. Graf *et al.* (1993)'s perpetual–January experiments showed that, when forced by the Pinatubo aerosol, the

ECHAM2 GCM produced a stronger–than–normal northern polar–night jet and stronger–than–normal zonal winds extending down to the troposphere. The Azores High was shifted northward with increased tropospheric westerly winds at 60°N and increased easterly winds at 30°N. Surface temperatures were higher than normal over northern Eurasia and North America. However, the 24–layer ST–GCM does not simulate the northern–hemisphere polar–night jet well (see Appendix A). This deficiency might have prevented the model from simulating correctly the dynamical responses of the atmosphere to the Pinatubo aerosol forcing near the North Pole in DJF. Third, the observed surface cooling in the Northern Hemisphere in JJA 1992 was mostly due to the direct radiative effect of volcanic aerosol, the back–scattering of solar radiation. There was less model dynamical responses involved in JJA than in DJF.

2. Atmospheric Temperature and Circulation Changes

The time evolutions of the global–mean monthly mean temperature anomalies for all layers of the standard model output from June 1991 through May 1993 are presented in Fig. 5.4 for the four experiments listed in Table 5.2, for the NCEP/NCAR Reanalysis, and for the difference between the Experiment SI:VOL+SSTA and the NCEP/NCAR Reanalysis. The NCEP/NCAR Reanalysis provides data only up to 10 hPa. For each set of ensemble experiments, the distributions of global–mean temperature anomalies simulated with the six different initial conditions are close to each other throughout the atmosphere (pictures not shown). We present only the ensemble means in Fig. 5.4. When the model is forced only by the Pinatubo aerosol, no matter with climatological SST (Fig. 5.4a) or with real–time SST (Fig. 5.4b) as boundary conditions, the simulated temperature increases in the stratosphere and decreases in the troposphere, and has little dependence on the type of SST used. A maximum warming of about 2.5°C is produced in the lower stratosphere during the middle of 1992. Fig. 5.4d shows that the influence of the SST anomalies on the simulated atmospheric temperature is small in the
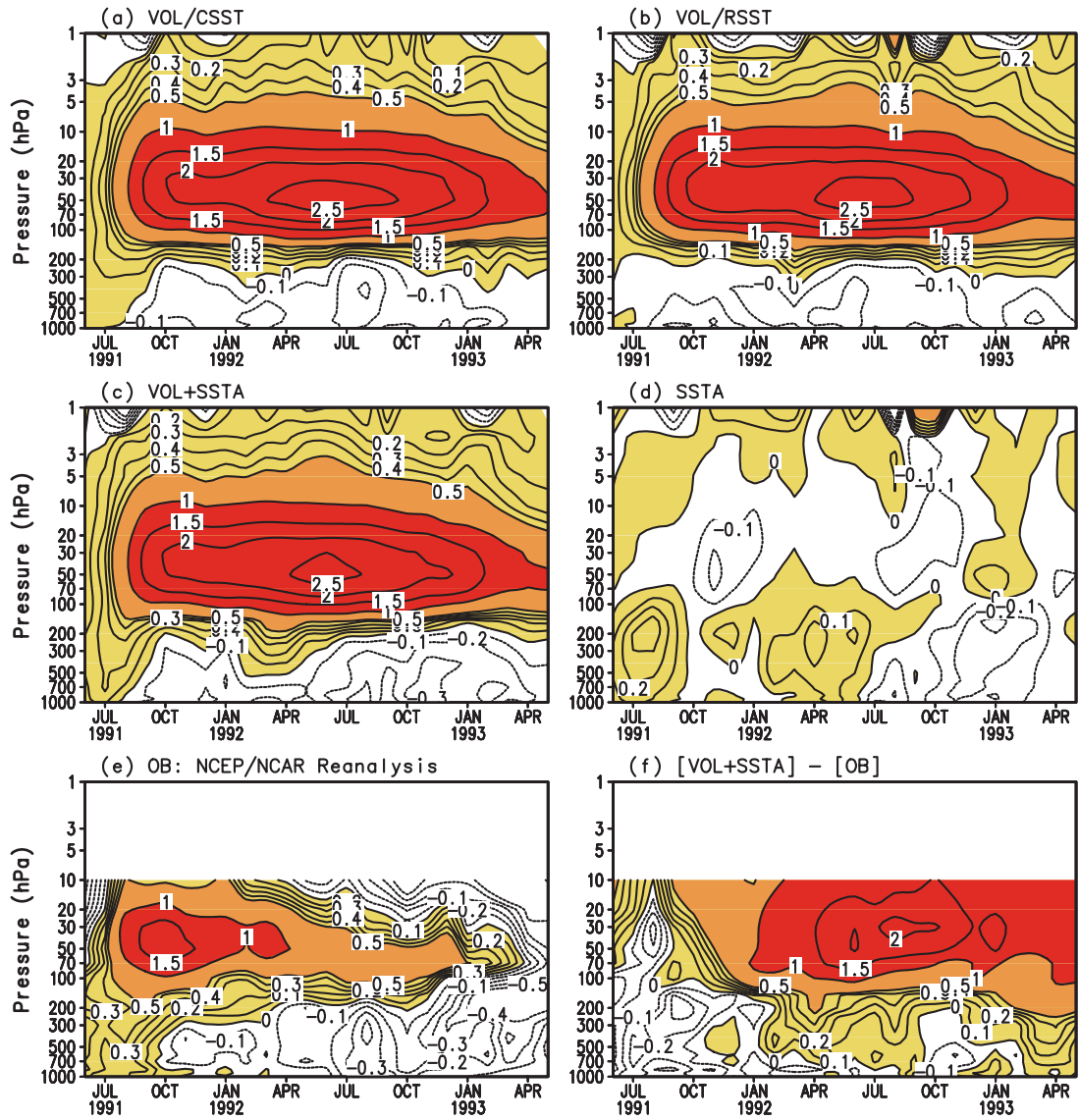
Fig. 5.4. *Time evolutions of global–mean temperature anomalies. Positive anomalies are shaded. The contour intervals are 0.1 for values between –0.5 and +0.5, and 0.5 for values beyond ±0.5.*

stratosphere, but comparable to that of the Pinatubo aerosol in the troposphere. When forced only by the SST anomalies (Fig. 5.4d), the simulated tropospheric temperature increases by 0.1°C to 0.3°C in JJA 1991 and MAM 1992, and decreases by 0.2°C in DJF 1992–1993. For the Experiment SI:VOL+SSTA (Fig. 5.4c), which includes both the Pinatubo aerosol forcing and the SST anomalies, the simulated temperature anomaly in the stratosphere is primarily caused by the Pinatubo aerosol forcing and looks like those in Fig. 5.4a and 4b, which include only the Pinatubo aerosol forcing. In the troposphere, the simulated temperature anomaly is produced by both the Pinatubo aerosol forcing and the SST anomalies, with the latter being more important. Kirchner and Graf (1995) also found in their perpetual–January simulations that El Niño signals can be more clearly detected in the troposphere than in the stratosphere, and that volcano signals are the strongest in the stratosphere.

Comparison between the temperature anomalies simulated by the Experiment SI:VOL+SSTA with the NCEP/NCAR Reanalysis (Fig. 5.4f) indicates that the model overestimated the observed warming in the lower stratosphere, but underestimated the observed cooling in the troposphere in 1992 and 1993. Large discrepancies up to +1.5°C ~ +2.0°C can be found during the middle of 1992 in the lower stratosphere. More experiments and data analyses will be presented in later sections to explain these discrepancies. It is noticeable that the model also slightly underestimated the observed warming in the lower stratosphere during a few months immediately after the Pinatubo eruption. This is probably because the prescribed aerosol optical properties accounted only for the sulfate aerosol particles but did not include the large amount of volcanic ash injected into the stratosphere. This ash returned to the earth's surface under gravitational settling in no more than a few months (McCormick *et al.* 1995). Volcanic ash can absorb upwelling terrestrial radiation and warm the lower stratosphere.

Fig. 5.5 shows the three–month–running–mean global–mean temperature anomalies for the four ensemble experiments listed in Table 5.2 and the NCEP/NCAR Reanalysis at 50 hPa and 500 hPa, respectively, for the two years following the Pinatubo eruption. At 50 hPa, the simulated temperature anomaly forced by SSTA is negligible. The simulated temperature anomalies from the other three ensembles are close to each other during the entire time period. They closely match the NCEP/NCAR Reanalysis during the first five months after the eruption, but are larger than the Reanalysis after November 1991. The largest discrepancy occurs in the middle of 1992. At 500 hPa, the observed global–mean temperature anomaly changed almost linearly from +0.35°C in June 1991 to about –0.12°C in December 1991. Both the volcanic forcing and the SST anomalies contributed to this rather steep temperature drop, with the latter being more important. The observed temperature increased a little bit between January and April in 1992, and then dropped to about –0.25°C in August 1992. Among all the experiments the temperature anomaly simulated by the Experiment SI:VOL+SSTA most closely matches the observed. The signal of volcanic forcing is weak. The Pinatubo eruption cooled the troposphere by 0.1°C to 0.15°C in the middle of 1992.

To better understand the latitudinal distributions of the simulated temperature anomalies, we present in Fig. 5.6 the latitude–time distributions of zonal–mean monthly mean temperature anomalies at 50 hPa from June 1991 through May 1993 for the NCEP/NCAR Reanalysis and for the four ensemble experiments listed in Table 5.2. For the NCEP/NCAR Reanalysis, values exceeding 1.3σ in magnitude are shaded, where σ is the standard deviation of the zonal–mean monthly mean temperature anomalies in the 1979–1995 time–period, which is the base–period used to derive the observed temperature anomalies. For the ensemble experiments, simulated temperature anomalies with statistical significance exceeding the 10% level for a two–tailed t–test are shaded.
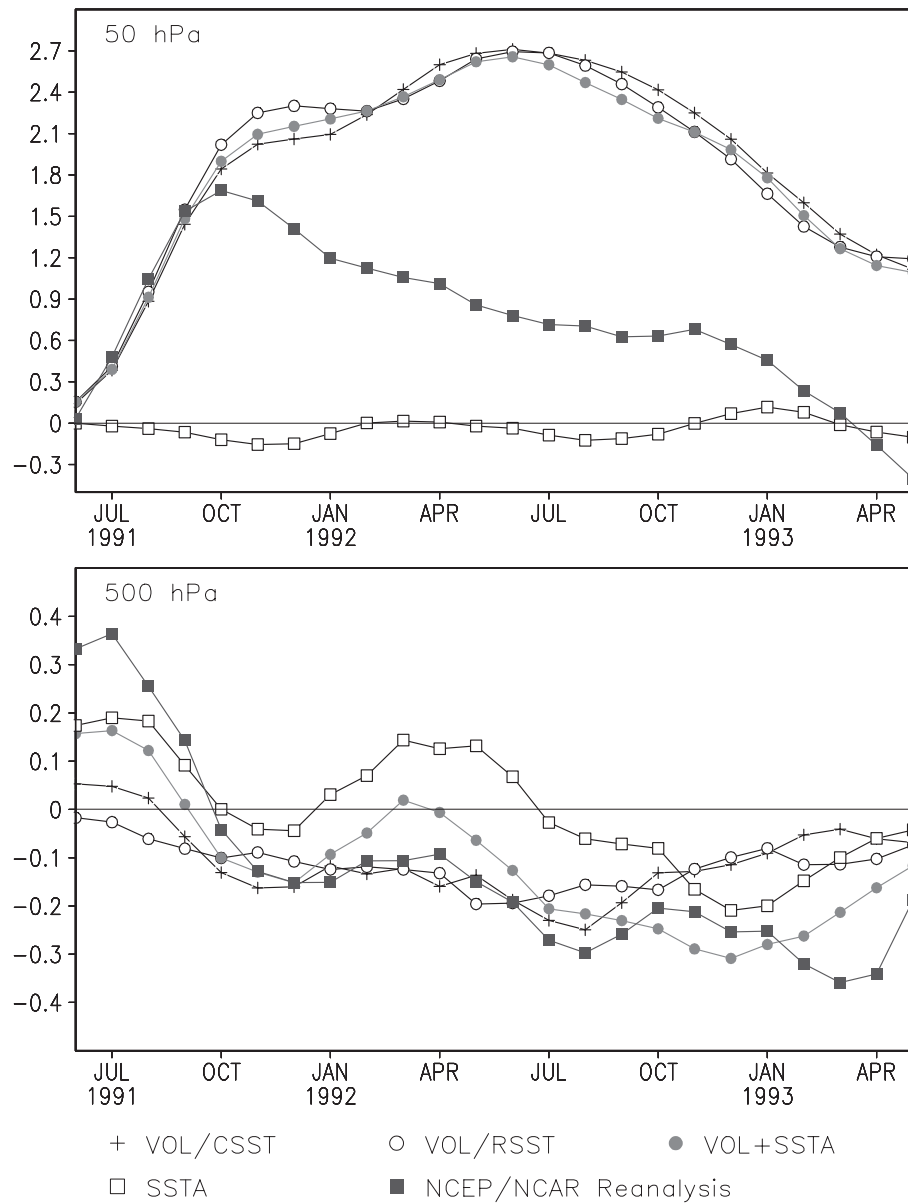
Fig. 5.5.   *Three–month–running–mean global–mean temperature anomalies at 50 hPa*

(upper panel) and 500 hPa (lower panel).

Fig. 5.6. *Time evolutions of monthly mean zonal–mean temperature anomalies at 50 hPa for (a) the NCEP/NCAR Reanalysis, and the simulations by the Experiments (b) SI:VOL+SSTA; (c) SI:VOL/CSST; (d) SI:VOL/RSST and (e) SI:SSTA. For the NCEP/NCAR Reanalysis, temperature anomalies larger than 1.3σ in magnitude are shaded, where σ is the standard deviation of zonal–mean temperature anomalies. For the simulations, areas with statistical significance exceeding the 10% level for a two–tailed t–test are shaded. The contour intervals are 1°C in (a), (b), (c) and (d), and 0.5°C in (e). Dashed lines are negative anomalies. Solid lines are positive anomalies.*
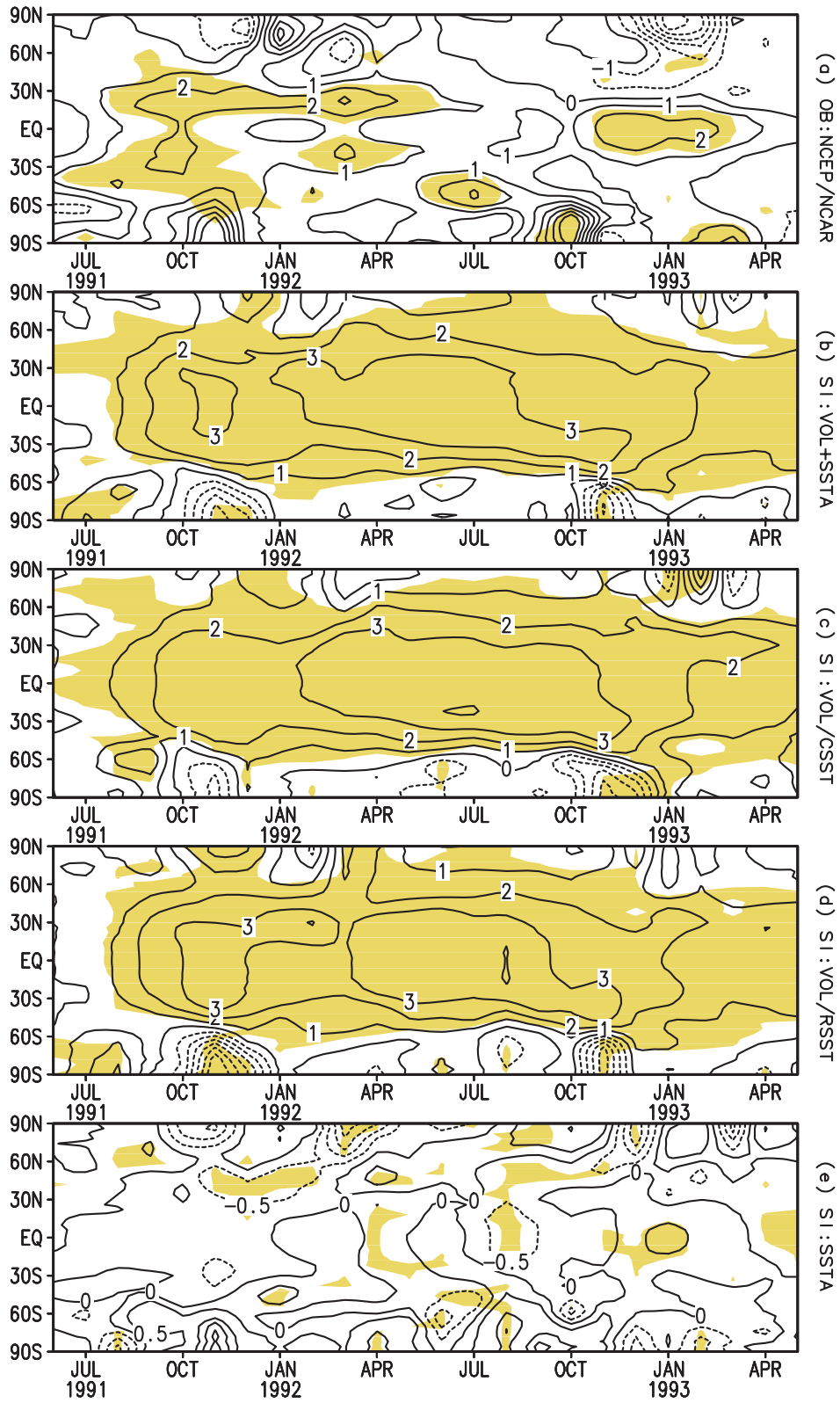
The observed temperature was about 1°C to 2°C higher than normal in the tropics and sub–tropics during most of the two years following the Pinatubo eruption. Between 10°N and 30°N a persistent and statistically significant large warming center existed from August 1991 through April 1992. In the tropics, the temperature anomaly was about +1°C to +2°C from August 1991 through March 1992, reduced to less than +1°C in the middle of 1992, and then increased again to about +2°C in DJF 1992–1993. The magnitude of the temperature anomalies in the tropics varied with time in part due to the dispersion of the Pinatubo aerosol clouds and in part due to the influence of the QBO (Angell 1997). In high latitudes, two strong warming centers up to +6°C occurred near the South Pole in November 1991 and October 1992 and a strong cooling center up to –6°C occurred near the North Pole in January 1993. These temperature anomalies have low statistical significance because the natural variability is large in the polar regions.

For the three ensemble experiments SI:VOL+SSTA, SI:VOL/CSST and SI:VOL/RSST, the simulated ensemble–mean temperature anomalies are significant everywhere except near the poles. The differences of temperature anomalies among the three ensembles are small at all latitudes and in all months except at the end of 1991 in the tropics, where the ensemble–mean temperature anomaly from experiment SI:VOL/CSST is about 1°C smaller than those from the other two experiments. The ensemble–mean temperature anomaly from the Experiment SI:VOL+SSTA matches the NCEP/NCAR Reanalysis a little better than the other two experiments. This occurs probably because that the Experiment SI:VOL+SSTA delineates more realistically the external forcings the real atmosphere had. In the subtropics and middle latitudes, the simulated temperature anomaly by the Experiment SI:VOL+SSTA is about +1°C larger than observed for all months. In the tropics, the simulated temperature anomaly is slightly larger than observed before January 1991, slightly smaller than observed after October 1992, and about 2°C larger than observed from February to September in 1992. More experiments and analyses will be

carried out in later sections to find out how much of these discrepancies can be explained by the influences of the QBO and the observed ozone depletion. For the Experiment SI:SSTA, the ensemble–mean temperature anomaly is everywhere less than ±0.5°C except near the poles, and is not significant. The signal of SST anomalies in the stratosphere is weak.

Kirchner *et al.* (1999) also performed ensemble simulations using the ECHAM4 GCM to examine the climatic impact of the Pinatubo eruption. When the model is forced only by the Pinatubo aerosol with climatological SST, the simulated ensemble–mean zonal–mean temperature anomaly is about 2~3°C larger than the NCEP/NCAR Reanalysis at 70 hPa, and about 1°C larger than that simulated by the UIUC 24–layer ST–GCM (Fig. 5.6c). We presented our results at 50 hPa because the simulated maximum warming by the 24–layer ST–GCM occurred for this layer. It is interesting to point out that the radiative forcing by the Pinatubo aerosol calculated by Stenchikov *et al.* (1998) (Fig. 8 of their paper), which was used by Kirchner *et al.* (1999), is about 2~3 W/m^2 smaller than that calculated by the UIUC 24–layer ST–GCM in the tropics where dense aerosol cloud occurred (see Figs. 3.6, 3.7 and 3.8, Chapter III), but the ECHAM4 GCM produced generally a larger warming than the UIUC 24–layer ST–GCM did in the tropics. It is possible that the ECHAM4 GCM is more sensitive to volcanic aerosol forcing than the UIUC 24–layer ST–GCM.

Fig. 5.7 presents the zonal–mean temperature anomalies at 500 hPa in the same format as in Fig. 5.6. Neither the simulated nor the observed temperature anomaly is everywhere statistically significant. For both the Experiment SI:VOL+SSTA and the NCEP/NCAR Reanalysis, warming occurred before July 1992 and cooling occurred after July 1992 in the tropics. By comparing the five figures in Fig. 5.7 with each other one can see that the temperature anomalies in the tropics simulated by the Experiment SI:VOL+SSTA are probably caused mainly by the SST anomalies instead of the Pinatubo aerosol forcing. In the middle and high latitudes,
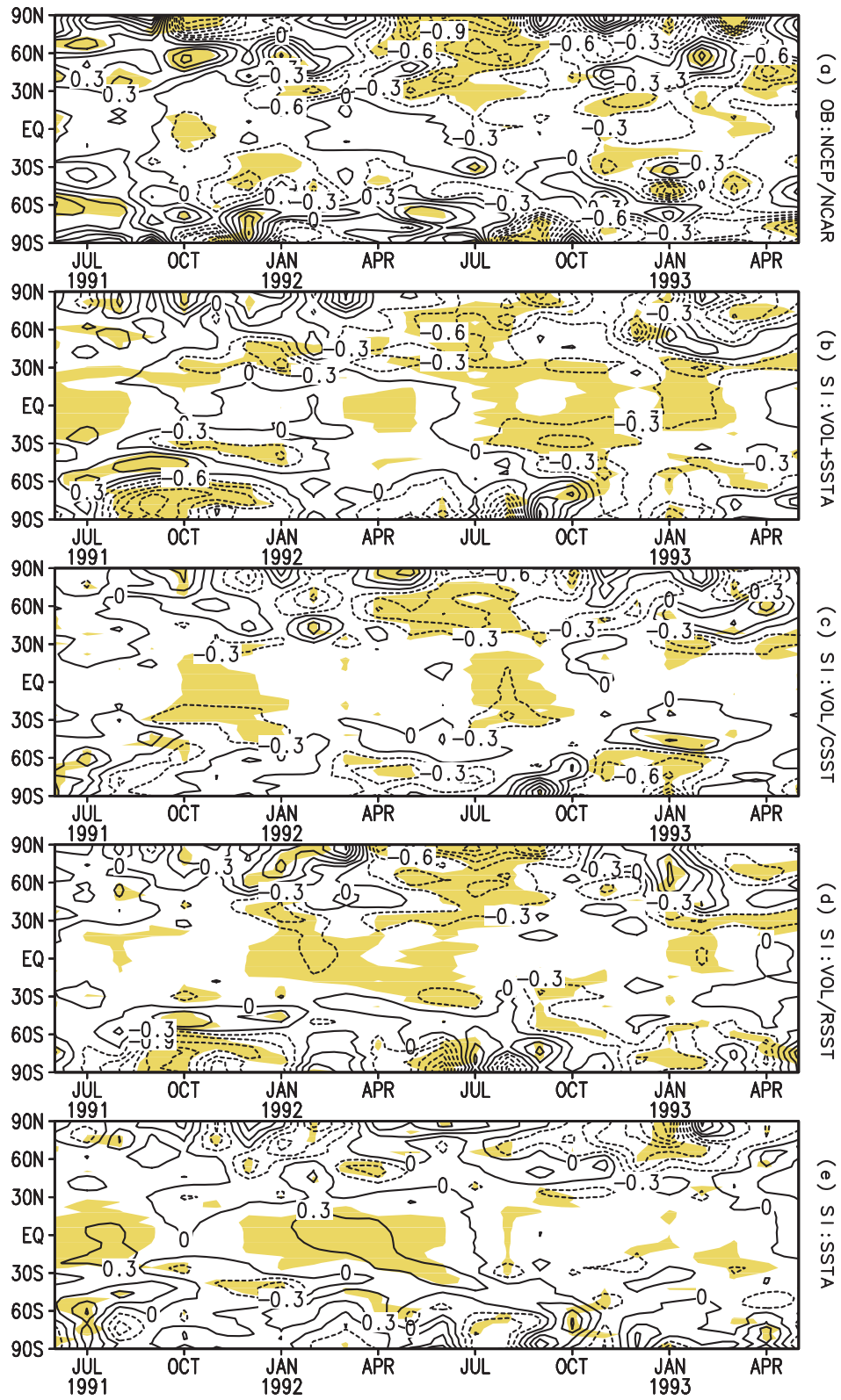
Fig. 5.7. *As in Fig. 5.6, except for temperature anomalies at 500 hPa.*

both the simulated and observed temperature anomalies exhibit large variations in time and latitude, and are insignificant most of the time. For all three ensemble experiments with the Pinatubo aerosol included, and also for the NCEP/NCAR Reanalysis, an area of negative temperature anomalies with high statistical significance is found in the northern–hemisphere middle to high latitudes from April to August in 1992. This cooling is probably caused by the back–scattering of solar radiation by aerosol clouds in the stratosphere.

How did the model simulate the atmospheric circulation when forced by the Pinatubo aerosol forcing and the SST anomalies? In Chapter IV, we analyzed the observed anomalies of seasonal–mean zonal–mean zonal wind from SON 1991 through JJA 1993 (Fig. 4.2) and found that the largest change of zonal–mean zonal wind in high latitudes occurred in the Northern Hemisphere in DJF 1992–1993 with high statistical significance. In the lower stratosphere, the northern polar vortex was about 10 m/s stronger than normal. In the troposphere, the zonal wind was also a few m/s stronger than normal. Fig. 5.8 shows the zonal–mean zonal wind anomalies in DJF 1992–1993 simulated by the four ensemble experiments listed in Table 5.2. None of the simulations that included the Pinatubo aerosol matches the observation in DJF 1992–1993 in Fig. 4.2f. The observed enhancement of the northern polar vortex was not captured. The model did not simulate the observed enhancement of the northern polar vortex in DJF 1991–1992 either (pictures not shown). In Appendix A we show that the vortex in the northern polar stratosphere in DJF simulated by the UIUC 24–layer ST–GCM is weaker than observed. This deficiency might have affected the model's dynamical response in the polar stratosphere to the Pinatubo aerosol forcing, and consequently the tropospheric circulation through the troposphere–stratosphere interaction (Kodera 1994). Nevertheless, Kirchner *et al.* (1999) showed that the observed changes of the northern polar vortex in DJF 1991–1992 and DJF 1992–1993 might not be necessarily

caused by the Pinatubo eruption. These changes might have resulted from the natural variability of the polar atmosphere.

Associated with the quasi–biennial oscillation of the equatorial zonal wind in the tropical lower stratosphere, there is a quasi–biennial oscillation of temperature (Angell 1997). However, the UIUC 24–layer ST–GCM is not able to simulate the QBO (Fig. A–19). In this chapter we estimate empirically the temperature anomalies in the tropical lower stratosphere associated with the QBO after the Pinatubo eruption using the NCEP/NCAR Reanalysis.
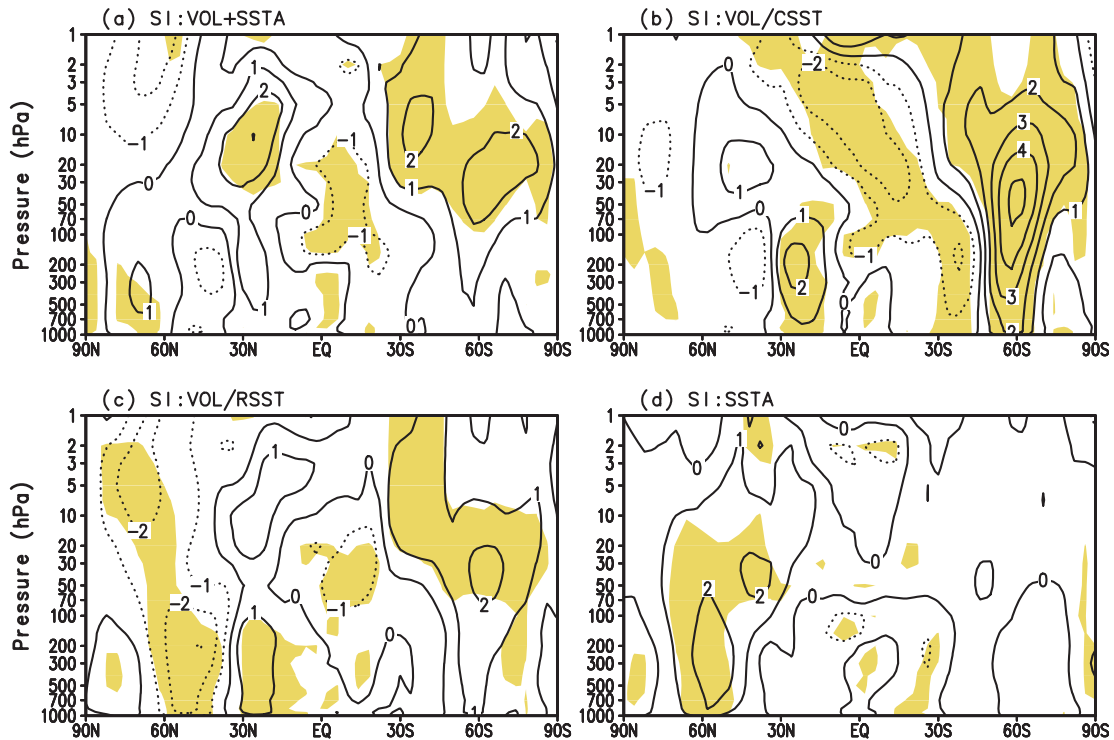
Fig. 5.8.   *Simulated zonal–mean zonal wind anomalies in DJF 1992–1993 by the Experiments (a) SI:VOL+SSTA, (b) SI:VOL/CSST, (c) SI:VOL/RSST, and (d) SI:SSTA. Solid lines are positive anomalies and dotted lines are negative anomalies. Areas with statistical significance exceeding the 10% level for a two–tailed t–test are shaded.*

D.   Influence of the QBO

We present in Fig. 5.9 the time evolutions of the monthly mean zonal–mean zonal wind at the equator between 70 hPa and 10 hPa, and the monthly mean zonal–mean temperature anomalies at 50 hPa between 30°S and 30°N from January 1958 through December 1998. The temperature anomalies are relative to the 1979–1995 climatology, and have been filtered by a high–pass filter with time scales less than 120 months. One can see that the zonal wind oscillates with a time period of about two years with its phase angle shifted downward from 10 hPa to 70 hPa with time. The filtered temperature anomaly also shows a quasi–biennial oscillation in the tropics with its phase angle slightly shifted with latitude. Abnormally large positive temperature anomalies can be seen following the volcanic eruptions of Agung, El Chichón and Mount Pinatubo. We analyze the averaged zonal–mean temperature anomalies between 12°S and 12°N.

The variation of the high–pass–filtered mean temperature anomalies between 12°S and 12°N at 50 hPa with time from January 1958 through December 1998 is plotted in Fig. 5.10a, together with the zonal–mean zonal wind at 30 hPa at the equator. The latter has been standardized and scaled to have the standard deviation of the temperature anomalies. We tested and found out that compared to those on other isobaric surfaces, the zonal wind at 30 hPa best matches the phase change of the temperature anomaly. The two time series exhibit a close correlation. A linear regression between the two time series is established by using the first 30 years of data from January 1958 through December 1987 (Fig. 5.10b). The regression correlation coefficient is 0.67, which exceeds the 0.1% level of statistical significance in light of the large freedom in the time domain. This statistical model, built on the linear regression, is then used to predict the temperature anomalies associated with the QBO after January 1988 by using the scaled zonal–mean zonal wind as predictor. Fig. 5.10c depicts the predicted QBO–related temperature anomalies at 50 hPa, averaged between 12°S and 12°N, for the two years following the Pinatubo
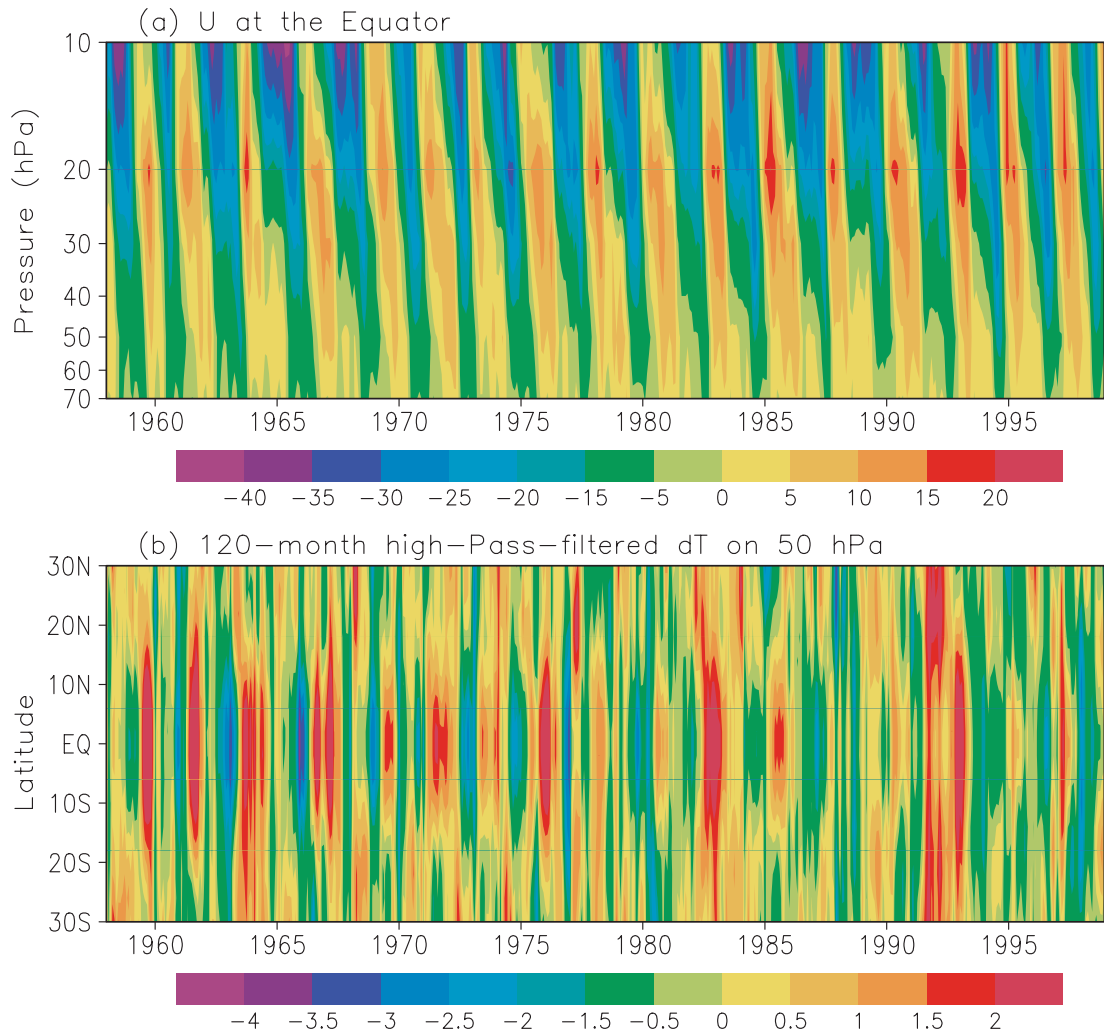
Fig. 5.9. *Time evolutions of (a) monthly mean zonal–mean zonal wind at the equator between 70 hPa and 10 hPa and, (b) the high–pass–filtered monthly mean zonal–mean temperature anomalies at 50 hPa between 30°S and 30°N from January 1958 through December 1998. Temperature anomalies are relative to the 1979–1995 climatology.*

Fig. 5.10. *(a). High–pass–filtered mean temperature anomalies between 12°S and 12°N at 50 hPa from January 1958 through December 1998, and the corresponding zonal–mean zonal wind at 30 hPa at the equator. The latter has been standardized and scaled to have the standard deviation of the temperature anomalies. (b). Scatter plot of the two time series in (a) using their first 30 years of data, and a linear regression. (c). mean temperature anomalies between 12°S and 12°N from June 1991 through May 1993 for the high–pass–filtered observation (OB:HPF), the prediction by the regression model (OB:QBO), the simulation by the ensemble Experiment VOL+SSTA (SI:VOL+SSTA), and the simulation adjusted to the QBO influence (Corrected SI:VOL+SSTA).*

(a) 12°S~12°N Mean ΔT at 50 hPa

Scaled U at the Equator at 30 hPa

(b) y = 0.0093772 + 0.71341x R= 0.66904

12°S~12°N Mean ΔT at 50 hPa

monthly data, 1958~1987

Scaled U at the Equator at 30 hPa

(c)

12°S~12°N Mean ΔT at 50 hPa (°C)

SI:VOL+SSTA

Corrected
SI:VOL+SSTA

OB:HPF

OB: QBO
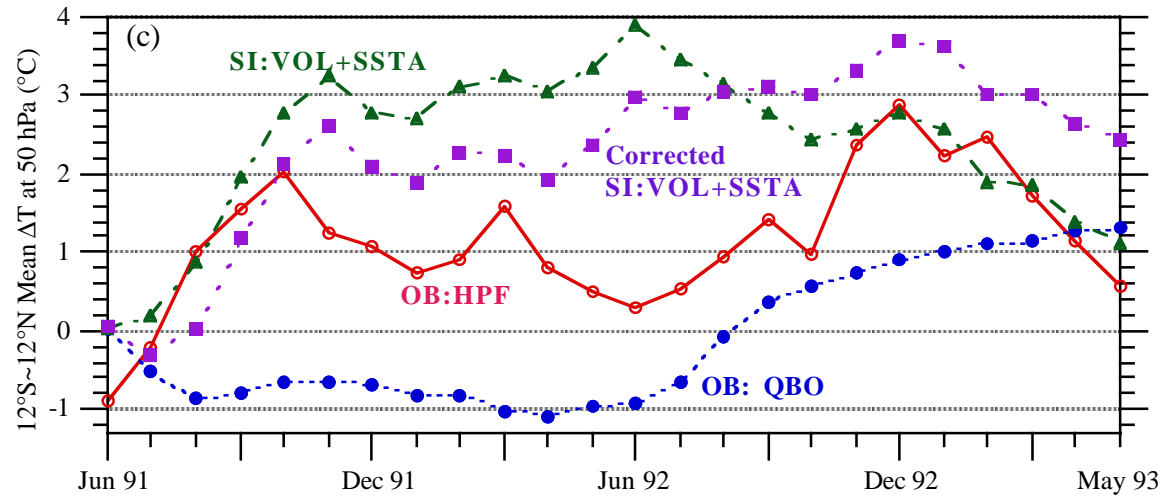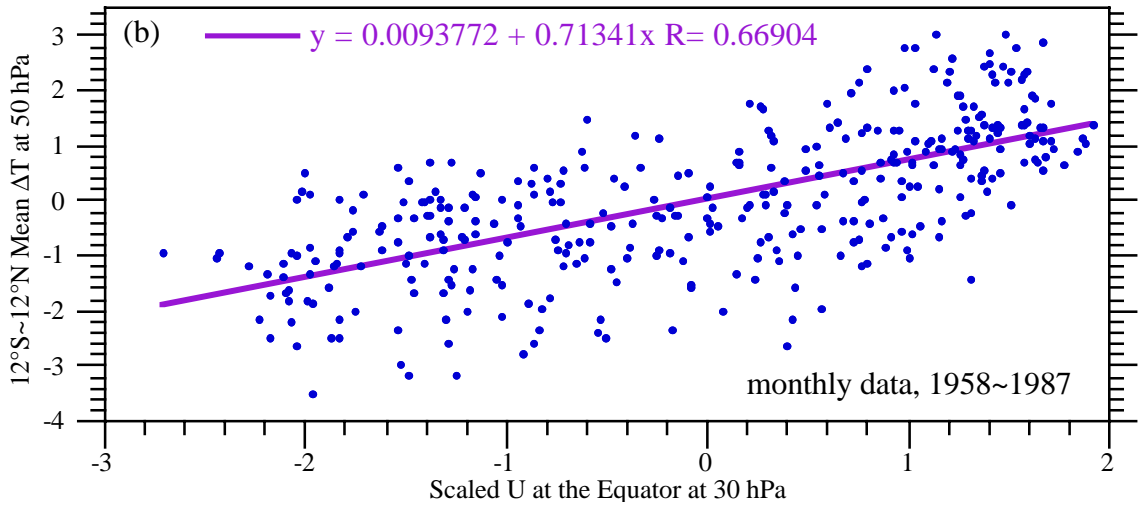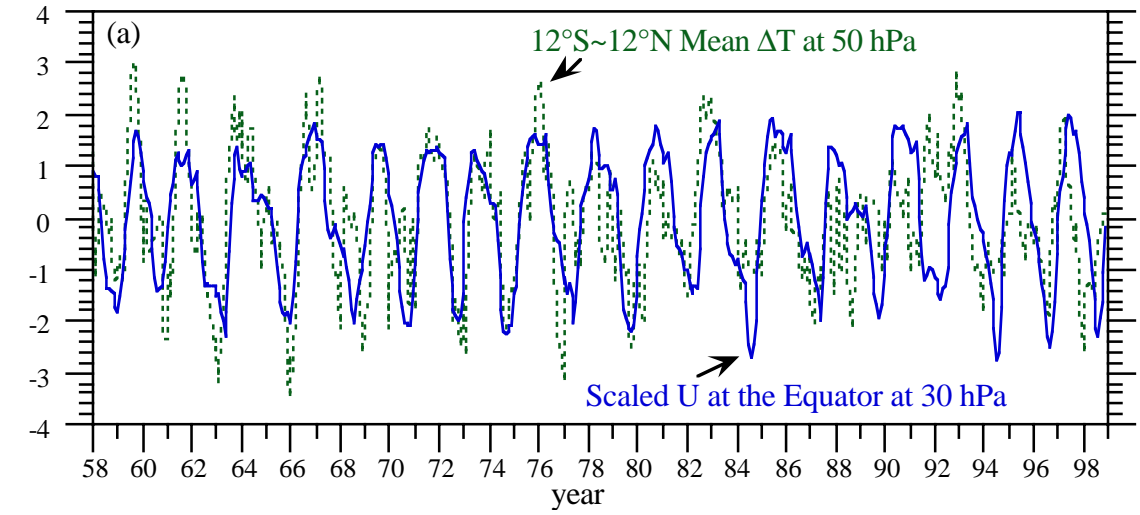
eruption, together with the observed high–pass–filtered temperature anomalies, the ensemble–mean temperature anomalies simulated by the experiment VOL+SSTA, and the ensemble–mean temperature anomalies after being adjusted to the QBO influence. The Pinatubo eruption occurred during a transition time of the QBO from a westerly phase to an easterly phase. Following the eruption, the QBO was in an easterly phase before JJA 1992 and in a westerly phase after JJA 1992 (Fig. 4.2). Correspondingly, the QBO–related temperature anomaly predicted by the linear regression model was about $-1.0°C$ before JJA 1992 and $1.0°C$ after JJA 1992. This QBO–related temperature oscillation explains in part the discrepancy between the observed and the simulated temperature anomalies in the tropical lower stratosphere. The remainder of the unexplained discrepancy is in part due to the ozone depletion caused by the volcanic aerosol.

E. Temperature Changes Induced by Ozone Depletion

Satellite observations revealed substantial total ozone losses over the globe for a few years following the Pinatubo eruption. Randel *et al.* (1995) showed that in the tropics, with the effect of the QBO excluded, the zonally averaged total ozone loss was initially about 4% in SON 1991, and about 2~3% throughout 1992 and 1993. In normal years, the column total ozone varies by ±2~4% in the tropics, almost synchronously with the quasi–biennial oscillation of the equatorial zonal wind (Bowman 1989). In the Northern Hemisphere poleward of 60°N, the observed zonal–mean total ozone decreased by about 10% during February–March 1992, by about 12% in February–March 1993 — extending from middle latitudes to the North Pole, and by about 4% throughout the rest of 1992 and 1993. In the Southern Hemisphere, large decreases of total ozone in excess of 10% were found in the high latitudes in the austral spring seasons for the three years following the Pinatubo eruption (Randel *et al.* 1995).

The Pinatubo volcanic aerosol was the major cause for these observed ozone losses. Several competing mechanisms were involved (Kinnison *et al.* 1994; Tie *et al.* 1994). First, the

absorption of solar and terrestrial radiation by the volcanic aerosol cloud radiatively warmed the atmosphere. This heating changed the atmospheric circulation, which in turn affected the meridional transport of trace gases, including ozone. Second, the backscattering of solar radiation by the aerosol cloud changed the photolysis rate of ozone, especially in the tropics. Third, the heterogeneous chemical reactions in the lower stratosphere were enhanced on the surface of the volcanic aerosol particles. The observed ozone losses after the Pinatubo eruption were primarily caused by the perturbations of the circulation and photolysis rate in the initial stage, and predominately by the enhanced heterogeneous chemical reactions in a later time, especially in the polar–night regions.

In the ensemble simulations performed by the 24–layer ST–GCM, the ozone concentration was prescribed in the model to equal the AMIP–II climatology. Ozone absorbs both solar radiation and terrestrial radiation. It is the major absorber of solar radiation in the stratosphere. To estimate the influence of the observed ozone depletion on the simulated atmospheric temperature, we need the distributions of ozone concentration changes resolved in space and time following the Pinatubo eruption. The observed column total ozone losses by satellites are not useful for GCM studies. Therefore, we performed two simulations by prescribing in the model the percentage changes of ozone concentration following the Pinatubo eruption simulated by two different 2–dimensional radiative–chemical–transport (RCT) models.

The first dataset of ozone concentration changes was simulated by Xue–Xi Tie (personal communication) using the NCAR 2–D RCT model and the method of Tie *et al.* (1994). This simulation spans June 1991 through May 1992. The effects of the Pinatubo aerosol on dynamical transport, photolysis rate and chemical reactions were included. The simulated ozone concentration changes were slightly modified to best reflect the Pinatubo eruption because the atmospheric circulation used in the 2–D model was that of 1985. Fig. 5.11 delineates the vertical

(a) O₃ Concentration Change (%) at 60N

(b) O₃ Concentration Change (%) at EQ

(c) O₃ Concentration Change (%) on 50 hPa (~20km)

(d) Total O₃ Change (%)
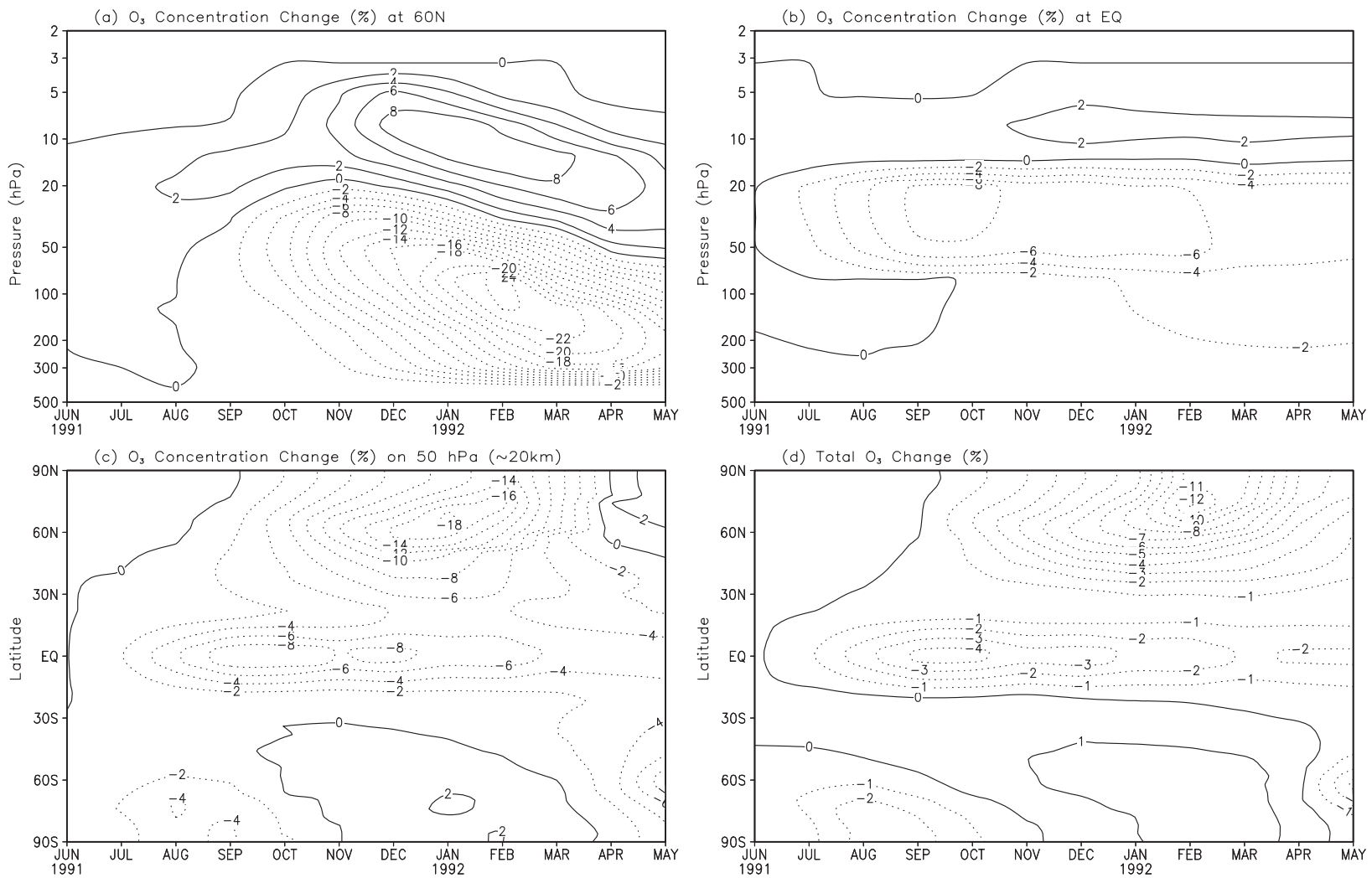
Fig. 5.11.   *Ozone depletion for the first year following the Pinatubo eruption simulated by Xue-Xi Tie (personal communication). Shown in (a), (b) and (c) are ozone concentration changes (%) at 60°N, at the equator and at 50 hPa, respectively, and in (d) the column-integrated total ozone changes (%).*

distributions at 60°N and at the equator, respectively, and the horizontal distribution at 50 hPa of the simulated percent changes of monthly mean ozone concentration from June 1991 through May 1992. The percent change of column–integrated total ozone is also presented in Fig. 5.11. The largest ozone depletion occurs in the northern lower polar stratosphere. The simulated total ozone losses near the North Pole in early 1992 and in the tropics in late 1991 match the observations (Randel *et al.* 1995) rather well. However, the model failed to simulate the observed ozone depletion in the Southern–Hemisphere high latitudes. The simulated maximum ozone loss near 60°N descended too fast with height, from about 50 hPa in October 1991 to about 150 hPa in March 1992.

The second dataset of ozone concentration changes was simulated by Kenneth Patten and Don Wuebbles (personal communication, hereinafter referred to as PW) using the Lawrence Livermore National Laboratory 2–D RCT model (Kinnison *et al.* 1994; Patten *et al.* 1994). They performed two 2–year–duration transient simulations, one with the aerosol surface area changing with time and the other with the aerosol surface area fixed to the value of 1990. In both simulations the atmospheric temperature and circulation were prescribed to be their climatological values, and were not allowed to respond to any external forcing. Therefore, the overloaded stratospheric aerosol following the Pinatubo eruption was allowed to affect only the heterogeneous chemical reactions. The simulated percent changes of ozone concentration and total ozone for the two years following the Pinatubo eruption are presented in Fig. 5.12 in the same format as in Fig. 5.11. This model captured the observed ozone losses in the Southern Hemisphere in the austral springs of 1991 and 1992 (Randel *et al.* 1995). In the Northern Hemisphere, the model also captured the observed large ozone losses in early boreal springs of 1992 and 1993. Probably due to the lack of dynamical responses, the simulated ozone depletion is almost everywhere larger than
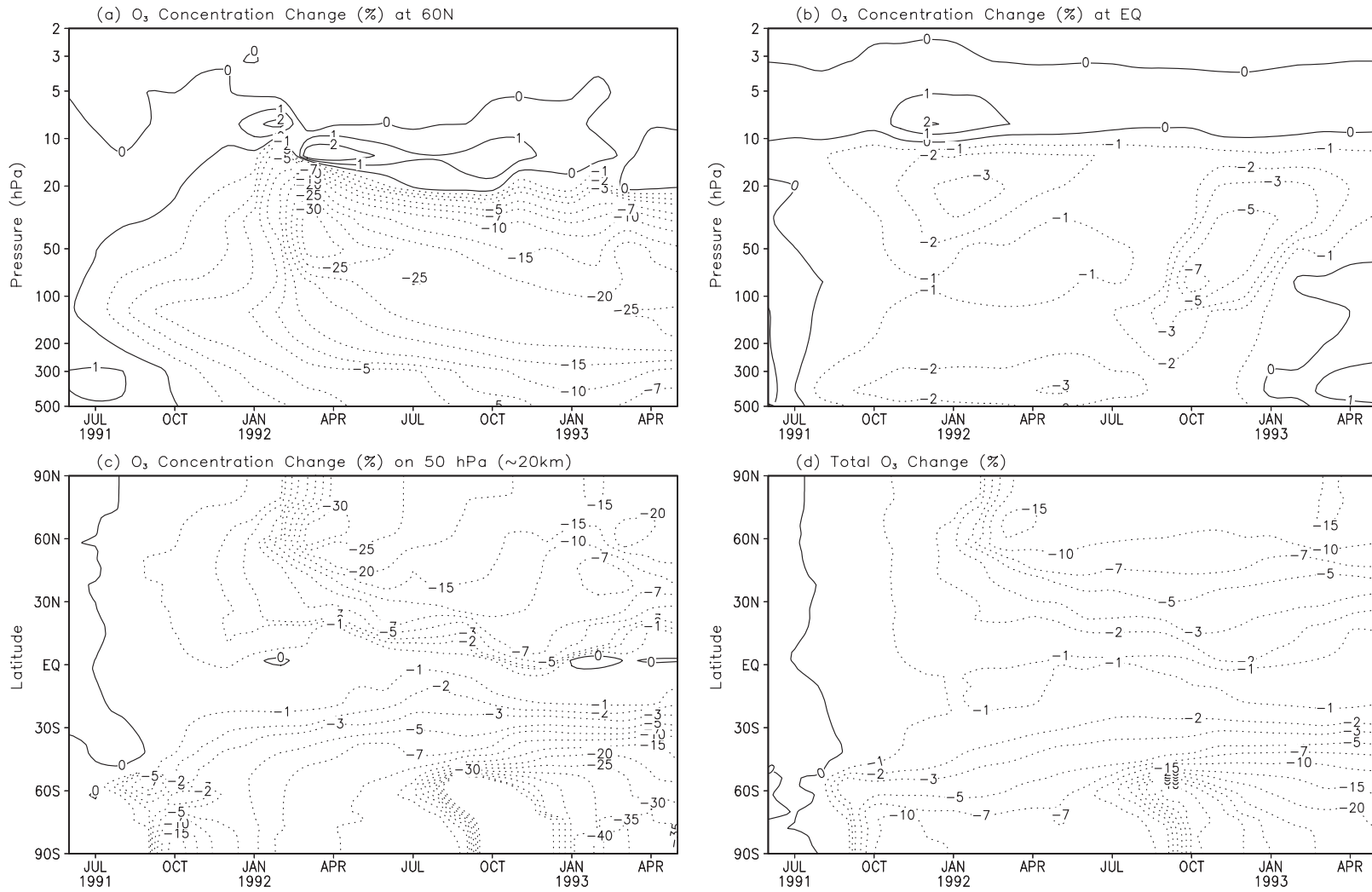
Fig. 5.12.   As in Figure 5.11, except for the ozone depletion for the two years following the Pinatubo eruption simulated by

Kenneth Patten and Don Wuebbles (personal communication).

observed, especially in the northern–hemisphere middle to high latitudes in 1992 summer. In the tropics, the simulated ozone losses are about 2~3% smaller than observed.

We performed two simulations, one from June 1991 to May 1992 and the other from June 1991 to May 1993, by prescribing in the UIUC 24–layer ST–GCM the percent changes of the zonally averaged ozone concentration simulated by the above 2–D RCT models. The simulations are compared to their corresponding control runs in Section C to estimate the influences of ozone depletion on the simulated temperature anomalies. We did not perform ensemble simulations here because the experiments in Section C showed that the simulated global–mean and zonal–mean temperature anomalies are not sensitive to the initial conditions in the stratosphere except near the poles. The time evolutions of the simulated temperature anomalies by these two experiments are presented in Fig. 5.13.

In the first simulation year, the simulated minimum global–mean temperature anomalies are about –0.2°C to –0.5°C with Tie's ozone data (Fig. 5.13a) and about –0.2°C with PW's ozone data (Fig. 5.13d) in the lower stratosphere at the end of 1991. In the first few months following the Pinatubo eruption, the simulated temperature anomalies at 50 hPa in the tropics with Tie's ozone data (Fig. 5.13b) are generally negative, and are about –0.5°C to –1.0°C; while the simulated temperature anomalies with PW's ozone data (Fig. 5.13e) are close to zero. This is because PW's simulation produced very small ozone depletion in the tropics. In both simulations, there is a minor warming in the tropics at 50 hPa in March and April 1992.

In the second simulation year from June 1992 to May 1993, the simulated global–mean temperature anomalies with PW's ozone data are almost everywhere –0.5°C between 30 hPa and 100 hPa, with the largest cooling of about –1.0°C occurring at the end of 1992. In the tropics at 50 hPa the simulated temperature anomalies are predominantly negative and vary from zero to –1.0°C. Near the poles the simulated temperature anomaly at 50 hPa varies from positive to
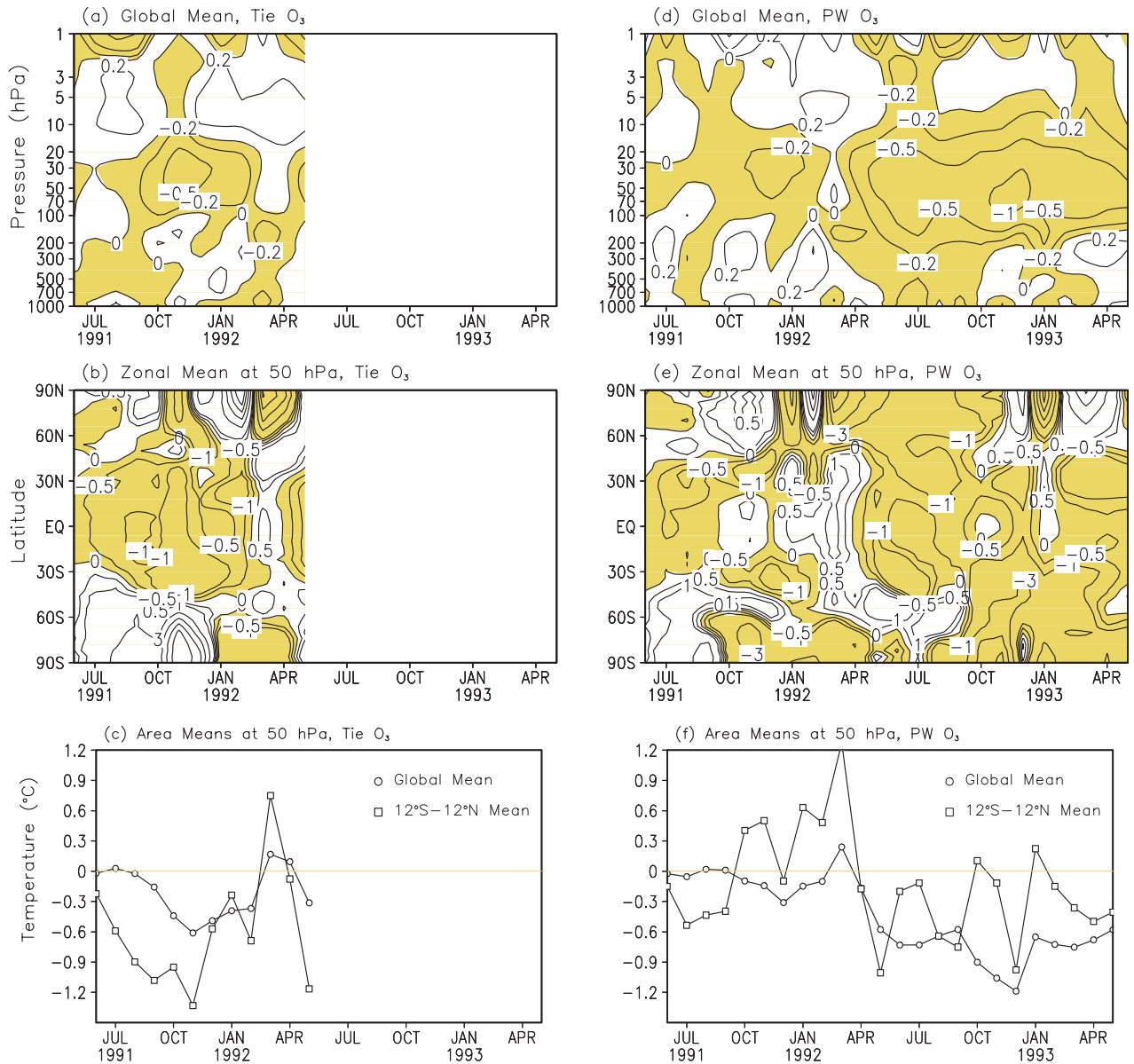
Fig. 5.13. *Temperature anomalies simulated by the 24-layer ST–GCM with prescribed ozone concentration changes from Tie (left panels) and Patten and Wuebbles (right panels). Shown in (a) and (d) are global means, in (b) and (e) are zonal means at 50 hPa, and in (c) and (f) are global means and the means between 12°S and 12°N at 50 hPa.*

 negative with large amplitude. As shown by the ensemble simulations in Fig. 5.6, the temperature anomalies simulated by the 24-layer ST–GCM are not statistically significant near the polar regions no matter what the forcing is.

Therefore, a large part of the discrepancy in the stratosphere, especially in the tropics and subtropics, between the observed temperature anomalies and the simulated temperature anomalies by the 24–layer ST–GCM with the Pinatubo aerosol forcing can be explained by the QBO–related temperature variations and the temperature changes induced by the ozone depletion following the Pinatubo eruption. However, there is still certain discrepancy that can not be explained, probably because the feedbacks among the QBO, ozone depletion and atmospheric temperature and circulation were not resolved, and the role of the ocean was not included.

F.   Influence of the Ocean

So far the 24–layer ST–GCM has been run with prescribed SSTs to study the climatic impact of the Pinatubo eruption. The influences of the oceanic thermal inertia and dynamics on the simulated atmospheric responses to the Pinatubo aerosol forcing have not been considered. In previous GCM studies on the climatic impact of the Pinatubo eruption, Hansen *et al.* (1996) coupled the GISS atmospheric GCM to a non–dynamic mixed–layer ocean model with diffusive heat transport to the deep ocean, while Graf *et al.* (1994) and Kirchner *et al.* (1999) used prescribed SSTs. In this section we use a coupled atmosphere–ocean GCM to simulate the climatic impact of the Pinatubo eruption.

The 24–layer ST–GCM has been coupled to an 18–layer oceanic GCM (OGCM). This OGCM was developed by Wang and Schlesinger (1998) based on a 6–layer OGCM (Han *et al.* 1985). It has 6 layers within the upper 120 m, and 12 layers within the upper 750 m; therefore, it possesses a better representation of the vertical structure of the oceanic boundary layer and the

thermocline than the 6–layer OGCM. While constant vertical viscosity and diffusivity were used in the 6–layer OGCM, Richardson–number–dependent viscosity and diffusivity are used in the 18–layer OGCM. The 18–layer OGCM has been integrated for 470 years with prescribed upper boundary conditions, and produced an improved model climatology compared with its previous versions (Wang and Schlesinger 1998). The coupled atmospheric and oceanic GCM was initialized from the 15th year of the uncoupled simulation of the 24–layer ST–GCM and the 470th year of the uncoupled simulation of the 18–layer OGCM. For spin–up, the coupled GCM was first integrated for 20 years without corrections in the simulated heat and water fluxes at the surface between the atmosphere and the ocean. During the integration the simulated sea–surface temperature (SST) and sea surface salinity (SSS) were compared to the observed climatological SST and SSS (Levitus 1994) to diagnose the restoring terms for the simulated heat and water fluxes. The coupled GCM was then run for 10 more years with corrections in the simulated heat and water fluxes by using the diagnosed monthly mean restoring terms averaged over the last 6 years of the first 20–year simulation.

For validation, the simulated monthly mean ocean temperature at (5°S, 120°W) in the upper 500 m and the simulated monthly mean SST between 150°E and 90°W at 5°S are presented in Fig. 5.14 for the last 6 simulation years with flux corrections, together with the observed climatological SSTs at 5°S (Levitus 1994). The oceanic mixed layer and the thermocline are already in quasi–equilibrium states. The coupled model simulates rather well the seasonal variation and magnitude of the SST in the tropical Pacific. The model simulates well the observed intrusions and recessions of the colder water in the eastern tropical Pacific in space and time. Fig. 5.15 shows the geographical distributions of annual–mean SSTs for the simulated SST averaged over the last 6 simulation years and for the observed climatological SST (Levitus 1994), and their
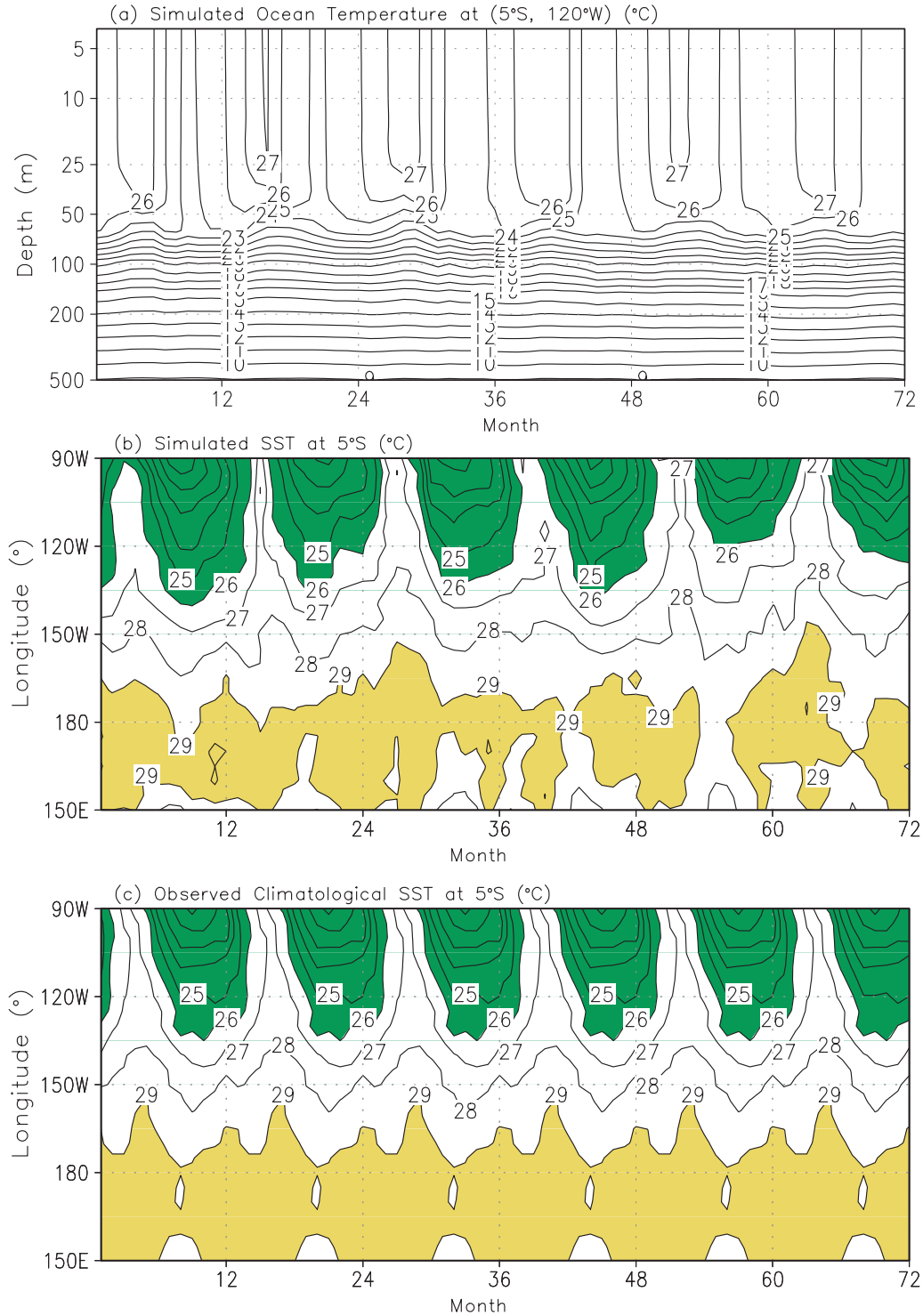
Fig. 5.14. *(a). Simulated monthly mean temperature (°C) in the upper 500 m of the ocean at (5°S, 120°W). (b). Simulated monthly mean SST at 5°S between 150°E and 90°W. Temperatures above 29°C are heavily shaded and below 26°C are lightly shaded. (c). As in (b), except for the observed climatology of SST.*
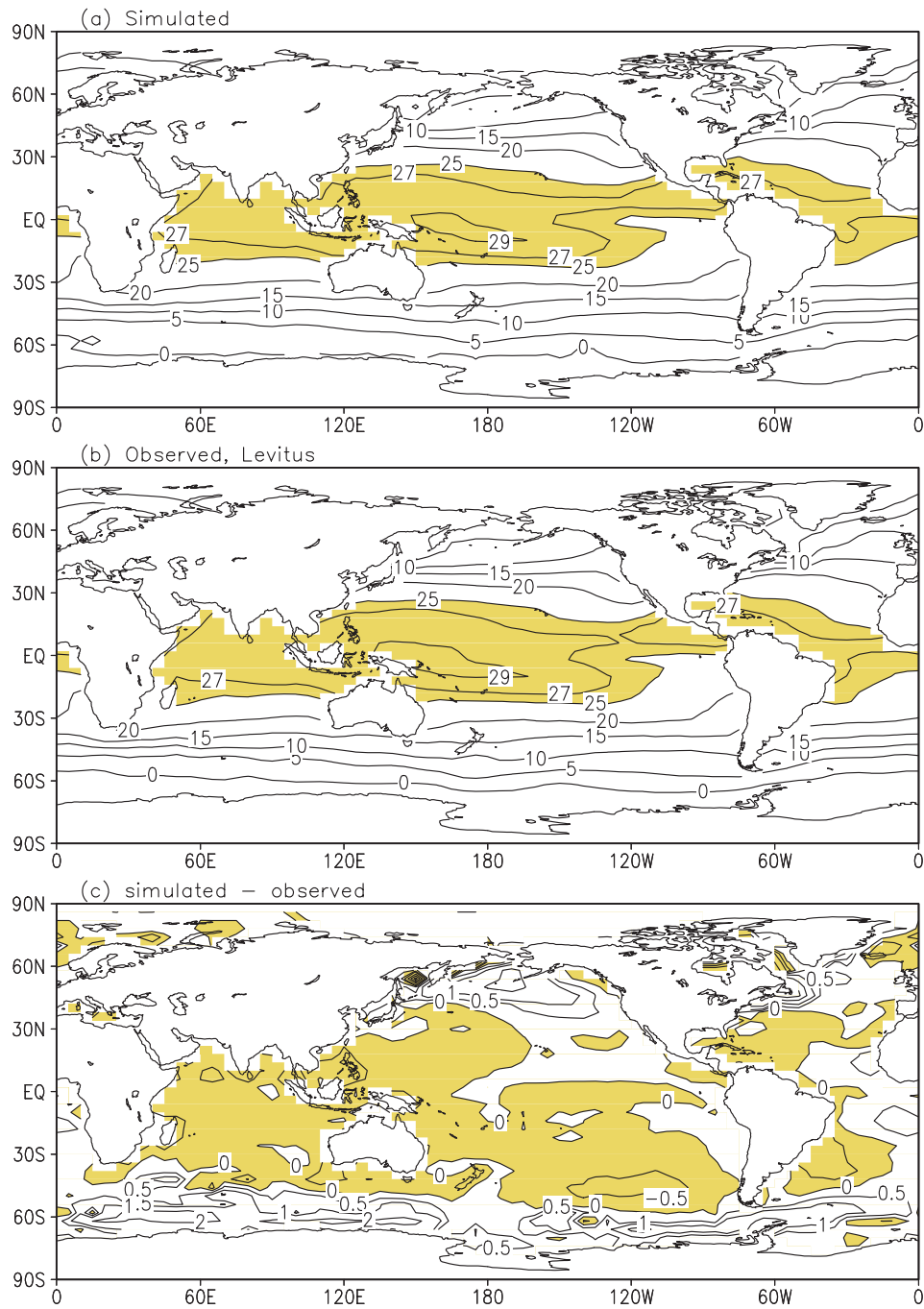
Fig. 5.15. *Annual–mean SSTs (°C) for (a) that simulated by the coupled GCM and (b) the observed climatology, and (c) the difference between the simulated and the observed SSTs. In (a) and (b) temperatures above 25°C are shaded. In (c) negative values are shaded.*

differences. The simulation is rather accurate in the tropics and lower latitudes, with errors less than ±0.5°C. Around Antarctica and in the northwestern Pacific and northwestern Atlantic the simulated SSTs are 1°C to 2°C warmer than observed.

To explore the influence of the ocean on the simulated responses of the atmosphere to the Pinatubo eruption, we performed six simulations using the coupled GCM with flux corrections. For each simulation the model was integrated for two years with the Pinatubo aerosol included in the atmosphere. Initial fields for the atmosphere and ocean models were chosen from the last 10–year spin–up integration of the coupled GCM with flux corrections. Each simulation was compared to its corresponding control run, the spin–up integration, to derive anomalous fields.

Fig. 5.16 presents the ensemble–mean surface–air temperature anomalies in DJF 1991–1992 and JJA 1992 simulated by the coupled GCM. Temperature anomalies with statistical significance exceeding the 10% level are shaded. For the simulation in DJF 1991–1992, the coupled GCM captured the observed warming (Fig. 5.2b) over central North America and the cooling over Africa, as did the uncoupled ST–GCM (Fig. 5.2a). Furthermore, the coupled model simulated the observed warming over northern central Eurasia, while the uncoupled ST–GCM did not. Graf *et al.* (1993) stated that the observed winter warming over both North America and Eurasia are related to the observed stronger–than–normal northern polar stratospheric vortex, which might have been caused by the anomalous radiative heating in the tropical lower stratosphere by the Pinatubo volcanic aerosol. However, the coupled GCM did not simulate a stronger–than–normal northern polar vortex (pictures not shown), neither did the uncoupled ST–GCM. The reason why the coupled GCM simulates the observed warming over northern central Eurasia is still unknown. For the simulation in JJA 1992, the coupled GCM captured the observed cooling (Fig. 5.3b) over North America, southern Eurasia and North Africa, as did the uncoupled ST–GCM (Fig. 5.3a). The coupled GCM simulated the observed cooling over northern

Eurasia better than the uncoupled ST–GCM. The simulated JJA–1992 cooling averaged over Eurasia, North America, South America and Africa is –1.1°C by the coupled GCM, and –0.5°C by the uncoupled ST–GCM. The observed cooling is –0.7°C. The overestimate of cooling by the coupled GCM is largest in North Africa.
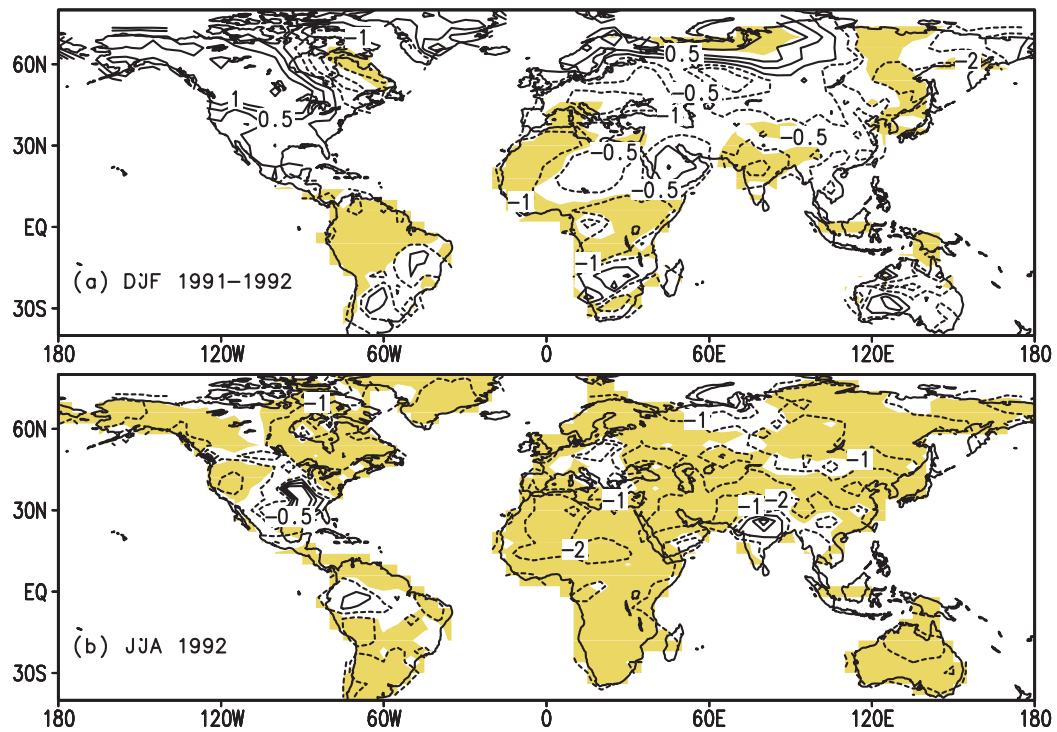
Fig. 5.16. *Ensemble–mean surface–air temperature anomalies in (a) DJF 1991–1992 and (b) JJA 1992 simulated by the coupled GCM. The contour interval is 1°C with the ±0.5°C lines added. Values with statistical significance exceeding the 10% level are shaded.*

Fig. 5.17 shows the ensemble–mean zonal–mean temperature anomalies at 50 hPa and 500 hPa, respectively, simulated by the coupled GCM for the two years following the Pinatubo eruption. The simulated stratospheric warming in the tropics and mid–latitudes is statistically significant and closely matches the stratospheric warming simulated by the uncoupled ST–GCM in magnitude and time (Fig. 5.6b). Globally averaged, the simulated stratospheric warming at 50 hPa in 1992 and 1993 by the coupled GCM is about 0.2°C to 0.3°C smaller than that simulated by the uncoupled ST–GCM. At 500 hPa, the coupled ST–GCM largely overestimated the observed cooling in the tropics and mid–latitudes in 1992 and 1993. The overestimate of the tropospheric cooling is probably because the sea–surface temperature in the Pacific simulated by the coupled GCM with the Pinatubo aerosol forcing in 1992 and 1993 is too cold compared to the SST in the control runs without the Pinatubo aerosol forcing, especially in the North Pacific (pictures not shown). The simulated SST anomalies in the eastern tropical Pacific are generally negative. The coupled model did not simulate the observed SST increases in the eastern tropical Pacific, the 1991–1992 and 1993 El Niños. Handler and Andsager (1993) hypothesized that all El Niño events are triggered by volcanic eruptions. The simulations performed here by the coupled GCM can not prove or disprove this hypothesis. This coupled model has a coarse horizontal resolution of 4°x5° for both the atmospheric and oceanic components. It is probably unable to simulate El Niño events in the tropical Pacific, regardless of whether these events are caused by external forcing or the internal variation of the ocean–atmosphere system.
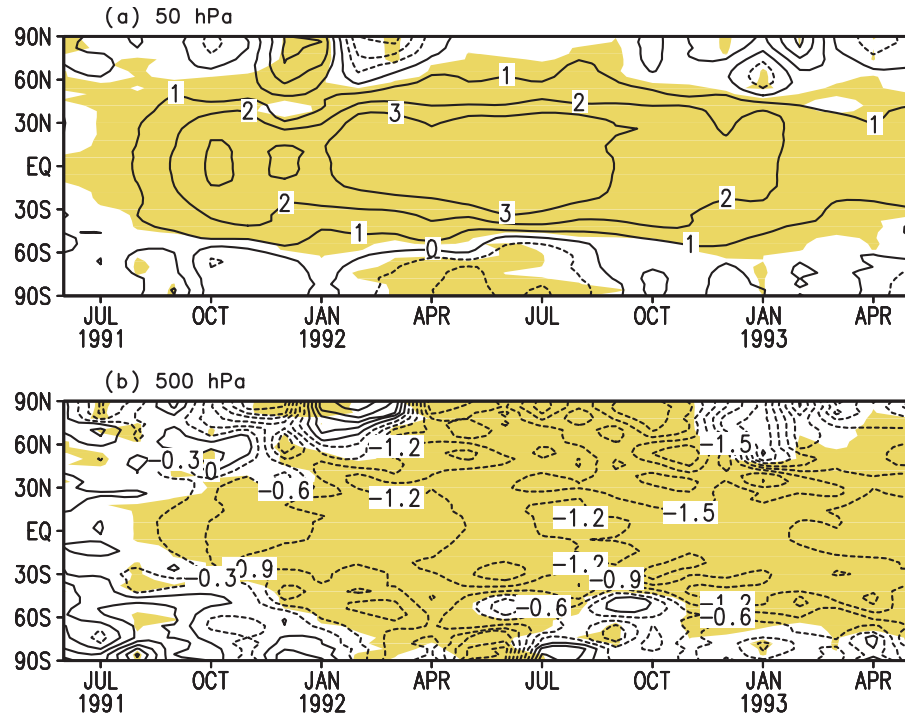
Fig. 5.17.   *Zonal–mean temperature anomalies at (a) 50 hPa and (b) 500 hPa simulated by the coupled GCM. The contour intervals are 1°C in (a) and 0.3°C in (b). Values with statistical significance exceeding the 10% level are shaded.*

G.   Summary

Using the UIUC 24–layer ST–GCM, we performed four sets of ensemble simulations to explore the thermal and dynamical responses of the atmosphere to the Pinatubo aerosol forcing for the two years following the Pinatubo eruption. The model captured the observed surface warming in DJF 1991–1992 and DJF 1992–1993 over central North America and the observed surface cooling in JJA 1992 over both North America and Eurasia. The model did not capture the observed warming in DJF 1991–1992 over Eurasia. The simulated ΔT_s are rather sensitive to the initial conditions, and vary with the type of SSTs prescribed in the model. Overall, the simulation

that is forced by both the Pinatubo aerosol forcing and the observed SST anomalies best matches the observations. The simulation that is forced by only the SST anomalies reproduces well the observed surface–air temperature anomalies over land that can be attributed to the ENSO effect from the SVD analysis in Chapter IV.

In the stratosphere, the model simulated the observed warming caused by the Pinatubo aerosol. The simulated temperature anomalies are not sensitive to initial conditions everywhere except near the poles. The magnitude of the simulated warming does not depend on the type of prescribed SSTs. The signal of SST anomalies is rather weak in the stratosphere. The 24–layer ST–GCM did not simulate the observed stronger–than–normal northern polar vortex in DJF 1991–1992 and DJF 1992–1993, probably because of the model's deficiency in simulating the northern polar vortex. In the troposphere, the model captured the observed cooling. The simulated temperature anomalies are rather sensitive to initial conditions and the type of prescribed SSTs. The signal of SST anomalies is stronger than the signal of the Pinatubo aerosol forcing in the troposphere.

In the lower stratosphere, the simulated temperature anomalies are about 1°C to 2°C larger than observed in the tropics and subtropics in late 1991 and 1992. Most of the discrepancy can be explained by the observed QBO–related temperature variation and the temperature changes induced by the observed ozone depletion. The NCEP/NCAR Reanalysis showed that the equatorial zonal wind changed from easterly wind to westerly wind in the fall of 1992 along with the phase change of the QBO. In the tropical lower stratosphere, the observed warming by the Pinatubo aerosol was diminished by up to 1°C before August 1992 and enhanced by up to 1°C after August 1992 by the QBO–related temperature changes. During the three years following the Pinatubo eruption, the column–integrated ozone observed by TOMS (Total Ozone Mapping Satellite) (Randel *et al.* 1995) decreased by 2% to 4% in the tropics and more than 10% in the high

latitudes in both hemispheres in late winter and early spring times. Two simulations were performed using the 24–layer ST–GCM with prescribed zonal–mean percent changes of ozone concentration simulated by two different two–dimensional radiative–chemical–transport models. Globally averaged, the ozone depletion induced by the Pinatubo eruption cooled the lower stratosphere by 0.2°C to 0.5°C in the first year following the Pinatubo eruption, and by 0.5°C to 1.0°C in the second year following the Pinatubo eruption.

Ensemble simulations were performed by the coupled 24–layer–atmosphere and 18–layer–ocean GCM to examine the influences of the ocean on the simulated atmospheric responses to the Pinatubo aerosol forcing. The coupled model better simulates the observed surface–air temperature anomalies over Eurasia than the uncoupled 24–layer ST–GCM does. The simulated stratospheric temperature anomalies are close to those simulated by the uncoupled 24–layer ST–GCM. This coupled model did not reproduce the observed abnormally high sea–surface temperature in the eastern tropical Pacific in 1991 and 1992. The coupled model produced a too cold troposphere when forced by the Pinatubo aerosol. It would be more advantageous to use a coupled GCM with a horizontal resolution finer than 4°x5° to study the role of the ocean in the climatic impact of the Pinatubo eruption, and possibly to answer the volcano–ENSO hypothesis.